

Dynamics of Entanglement in One-Dimensional Spin Systems

Luigi Amico, Andreas Osterloh

MATISS-INFN & Dipartimento di Metodologie Fisiche e Chimiche (DMFCI), viale A. Doria 6, 95125 Catania, ITALY

Francesco Plastina, Rosario Fazio

NEST-INFN & Scuola Normale Superiore, I-56127 Pisa, ITALY

G. Massimo Palma

NEST-INFN & Dipartimento di Tecnologie dell'Informazione, Università degli studi di Milano via Bramante 65, I-26013 Crema(CR), ITALY

We study the dynamics of quantum correlations in a class of exactly solvable Ising-type models. We analyze in particular the time evolution of initial Bell states created in a fully polarized background and on the ground state. We find that the pairwise entanglement propagates with a velocity proportional to the reduced interaction for all the four Bell states. Singlet-like states are favored during the propagation, in the sense that triplet-like states change their character during the propagation under certain circumstances. Characteristic for the anisotropic models is the instantaneous creation of pairwise entanglement from a fully polarized state; furthermore, the propagation of pairwise entanglement is suppressed in favor of a creation of different types of entanglement. The “entanglement wave” evolving from a Bell state on the ground state turns out to be very localized in space-time. Further support to a recently formulated conjecture on entanglement sharing is given.

I. INTRODUCTION

A quantum mechanical system possesses additional correlations that do not have a classical counterpart. This phenomenon, called entanglement [1], is probably one of the most astonishing features of quantum mechanics. Understanding the nature of these non-local correlations has been a central issue in the discussion of the foundation of quantum mechanics. More recently, with the burst of interest in quantum information processing, entanglement has been identified as an ingredient for the speed-up in quantum computation and quantum communication protocols [2] as compared with their classical counterparts. Therefore it is of crucial importance to be able to generate, manipulate and detect entangled states and experimental efforts in this direction have been put forward. Notable results have been obtained with photons [3], cavity QED systems [4], ion traps [5], and coupled quantum dots [6]. Also encouraged by the advances in the field of nanoscience, there has been already a number of proposals to detect signatures of entanglement. Systems under current study are multiterminal mesoscopic devices [7] and Josephson junctions [8]. In many-body systems correlated states naturally appear. In fact a research activity investigating entanglement in condensed matter systems has been emerging very recently. Many aspects still need further investigation though. From a conceptual point of view, it is not always obvious for example, how to distill out the quantum part of the correlations since interaction between the subsystems is always on. Nevertheless many-body systems might become useful for the development

of new computation schemes and/or communication protocols. As an example we mention the recent proposal by Bose [9] to use the spin dynamics in Heisenberg rings to transfer quantum states. It is conceivable that along the same lines other quantum information tasks can be implemented as well.

An important motivation for us to study the interconnection between condensed matter and quantum information is to investigate whether it is possible to better characterize condensed matter states by looking at the entanglement properties of their wavefunction. To realize such a program, tools of quantum information theory can be applied [10]. Already a number of interesting results in this direction have been obtained for systems of interacting spins. In the Heisenberg chain the maximization of the entanglement at zero temperature is related to the energy minimization [11] while at finite temperature violation of Bell's inequality can be directly related to the properties of the internal energy [12]. It is known that Werner states [13] can be generated in a one dimensional XY model [14] and that temperature and/or magnetic field can increase the entanglement of the systems as shown for the Ising and Heisenberg model in Refs. [15,16]. The peculiar aspects of non-local correlations become particularly evident when many bodies behave collectively, a prominent example being a system near a quantum phase transition [17]. It was found that near a quantum phase transition entanglement can be classified in the framework of scaling theory [18–21], but also profound differences between non-local quantum and classical correlations have been highlighted. In a very recent paper the problem of decoherence in a near-critical

one-dimensional system was addressed [22].

The analysis of the entanglement was not confined to spin systems. Attention has also been devoted to the BCS model [23,24], quantum Hall [25] and Boson systems [26].

The link between statistical mechanics and quantum information theory has been carried ahead in refining established methods for examining many body interacting systems. An example is the entanglement preserving Density Matrix Renormalization Group introduced in Ref. [27]. In this paper we are interested in the dynamics of entanglement in one-dimensional systems. In condensed matter physics it is customary to analyze the behaviour of the system by creating an excitation in a given point and studying its time evolution. We follow this idea, creating a localized entangled state (typically a Bell state) and following the evolution of entanglement generated by the dynamics of the spin chain. There are a number of questions that can be addressed in this way. In particular we would like to see if there is a well defined velocity of propagation of entanglement, how it is related to the propagation of the elementary excitations of the spin system and what are the time scales for damping the entanglement created at the initial time.

The questions addressed in this paper may be relevant for the study of quantum limits to dynamical evolution [28]. Entanglement, indeed, allows to achieve the quantum mechanically accessible speed maximum in the evolution of a composite system towards orthogonal states. Finally, an important aspect we address in our analysis is to discriminate pairwise from different types of entanglement. This problem was quantified by Coffman, Kundu, and Wootters (CKW) recently in terms of a conjecture [29] on a measure for residual entanglement that connects the pairwise entanglement between a certain spin and all others with the von Neumann entropy of this spin.

The paper is organized as follows: In the next section we will introduce the model Hamiltonian and describe briefly the techniques used to obtain the results (spectrum and correlation functions) discussed in the subsequent sections. In section III we discuss the measures of one- and two-site entanglement of formation and recall the CKW conjecture on the residual entanglement. The results for the isotropic and anisotropic models are presented separately in section IV. We will consider different initial states and different parameter ranges of the chosen model. The final section is devoted to the conclusions. Some details of the calculation are presented in the appendices.

II. THE MODEL

The system under consideration is a spin-1/2 ferromagnetic chain with an exchange coupling λ in a trans-

verse magnetic field of strength h . The Hamiltonian is $H = hH_s$ with the dimensionless Hamilton operator H_s being

$$H_s = -\lambda \sum_{i=1}^N (1+\gamma) S_i^x S_{i+1}^x + (1-\gamma) S_i^y S_{i+1}^y - \sum_{i=1}^N S_i^z \quad (1)$$

where S^a are the spin-1/2 matrices ($a = x, y, z$) and N is the number of sites. We assume periodic boundary conditions. The anisotropy parameter γ connects the quantum Ising model for $\gamma = 1$ with the isotropic XY model for $\gamma = 0$. In the interval $0 < \gamma \leq 1$ the model belongs to the Ising universality class and for $N = \infty$ it undergoes a quantum phase transition at the critical value $\lambda_c = 1$. The order parameter is the magnetization in x -direction, $\langle S^x \rangle$, which is different from zero for $\lambda > 1$ and vanishes at and below the transition. On the contrary the magnetization along the z -direction, $\langle S^z \rangle$, is different from zero for any value of λ .

This class of models can be diagonalized by means of the Jordan-Wigner transformation [30–32] that maps spins to one dimensional spinless fermions with creation and annihilation operators c_l^\dagger and c_l . It is convenient to use the operators $A_l \doteq c_l^\dagger + c_l$, $B_l \doteq c_l^\dagger - c_l$, which fulfill the anticommutation rules

$$\begin{aligned} \{A_l, A_m\} &= -\{B_l, B_m\} = 2\delta_{lm}, \\ \{A_l, B_m\} &= 0. \end{aligned} \quad (2)$$

In terms of these operators the Jordan-Wigner transformation reads

$$\begin{aligned} S_l^x &= \frac{1}{2} A_l \prod_{s=1}^{l-1} A_s B_s \\ S_l^y &= -\frac{i}{2} B_l \prod_{s=1}^{l-1} A_s B_s \\ S_l^z &= -\frac{1}{2} A_l B_l. \end{aligned} \quad (3)$$

The Hamiltonian defined in Eq.(1) is bilinear in the fermionic degrees of freedom and therefore can be diagonalized by means of the transformation

$$\eta_k = \frac{1}{\sqrt{N}} \sum_l e^{ikl} \left(\alpha_k c_l + i\beta_k c_l^\dagger \right) \quad (4)$$

with coefficients

$$\begin{aligned} \alpha_k &= \frac{\Lambda_k - (1 + \lambda \cos k)}{\sqrt{2[\Lambda_k^2 - (1 + \lambda \cos k)\Lambda_k]}} \\ \beta_k &= \frac{\gamma \lambda \sin k}{\sqrt{2[\Lambda_k^2 - (1 + \lambda \cos k)\Lambda_k]}}. \end{aligned} \quad (5)$$

The Hamiltonian thereafter assumes the form

$$H = \sum_k \Lambda_k \eta_k^\dagger \eta_k - \frac{1}{2} \sum_k \Lambda_k \quad (6)$$

and the associated energy spectrum is

$$\Lambda_k = \sqrt{(1 + \lambda \cos k)^2 + \lambda^2 \gamma^2 \sin^2 k}.$$

The time evolution of the original spin operators (or equivalently of the spinless fermions introduced in Eq.(3)) are the key to determine the time evolution of the entanglement and can be found by means of the inverse of Eq.(4)

$$c_j(t) = \sum_l [\tilde{a}_{l-j}(t)c_l - \tilde{b}_{l-j}(t)c_l^\dagger]$$

where the new coefficients are

$$\tilde{a}_x(t) = \frac{1}{\sqrt{N}} \sum_k \cos kx (e^{i\Lambda_k t} - 2i\beta_k^2 \sin \Lambda_k t) \quad (7)$$

$$\tilde{b}_x(t) = \frac{2i}{\sqrt{N}} \sum_k \sin kx \alpha_k \beta_k \sin \Lambda_k t. \quad (8)$$

In the limit $\gamma = 0$ the previous expressions simplify considerably. In this case the magnetization, i.e. the z -component of the total spin $S^z = \sum_j S_j^z$, is a conserved quantity. In terms of fermions this corresponds to the conservation of the total number of particles, $N = \sum_j n_j = \sum_j c_j^\dagger c_j$. For $\gamma \rightarrow 0$ and $|\lambda| \leq 1$ we find that $\alpha_k \rightarrow 0$ and $\beta_k \rightarrow \text{sign } k$. The energy spectrum is $\Lambda_k = |1 + \lambda \cos k|$ and the eigenstates are plane waves (the Hamiltonian corresponds to a tight binding model)

$$c_j(t) = \frac{1}{\sqrt{N}} \sum_k \sum_l \cos k(l-j) e^{-i\Lambda_k t} c_l \quad (9)$$

$$\eta_k^\dagger = \frac{1}{\sqrt{N}} \sum_l e^{-ikl} c_l. \quad (10)$$

A. Correlation functions

As specified within the next section, one- and two site-entanglement measures are obtained from the (one- and two-body) reduced density matrix whose entries can be related to various spin correlation functions

$$M_l^\alpha(t) = \langle \psi | S_l^\alpha(t) | \psi \rangle \quad (11)$$

$$g_{lm}^{\alpha\beta}(t) = \langle \psi | S_l^\alpha(t) S_m^\beta(t) | \psi \rangle. \quad (12)$$

These can be recast in the form of Pfaffians [32,33]. Correlators defined in Eq.(12) have been calculated for this class of models in the case of thermal equilibrium [30–32,34]. In this case, the expression for the correlators reduces to the calculation of Toeplitz determinants

(i.e. determinants, whose entries depend only on the difference of its row and column number). In the present work we are interested in calculating averages and correlation functions in the chain as a function of time for a given initial state $|\psi\rangle$ at time $t_0 = 0$, which is not an eigenstate of the Hamiltonian of Eq.(1). Therefore, the Pfaffians [35] do not reduce to Toeplitz determinants. Since the Hamiltonian is time-independent all the observables depend on the difference $t - t_0 = t$. Details of the calculations are reported in Ref. [36].

In order to grasp the properties associated to the dynamics of entanglement, we will always imagine that an initial configuration is prepared in which the entanglement is concentrated between two sites in the chain. The simplest situation to imagine is that two sites are in a Bell state and the rest of the chain is factorized with all spins in the state $|\downarrow\rangle$ (or $|\uparrow\rangle$)

$$\begin{aligned} |\Psi_{i,j}^\varphi\rangle &\equiv \frac{1}{\sqrt{2}} (|\downarrow, \dots, \downarrow \uparrow \downarrow \dots, \downarrow\rangle_N + e^{i\varphi} |\downarrow, \dots, \downarrow \uparrow \downarrow \dots, \downarrow\rangle_N) \\ &= \frac{1}{\sqrt{2}} (c_i^\dagger + e^{i\varphi} c_j^\dagger) |\downarrow\rangle \end{aligned} \quad (13)$$

where the vacuum state is defined as $|\downarrow\rangle = |\downarrow \dots \downarrow\rangle$. We notice again that the translational invariance is broken since the result for the wavefunction (13) in (12) depends on the positions i and j . The correlators $\langle \Psi_{i,j}^\varphi | S_l^\alpha S_m^\beta | \Psi_{i,j}^\varphi \rangle$ can be expressed as a *sum of Pfaffians* [36]

In the case $\varphi = 0, \pi$ ($|\Psi_{i,j}^\pi\rangle =: |-\rangle$ and $|\Psi_{i,j}^0\rangle =: |+\rangle$) it turns out that

$$\langle \pm | S_l^\alpha S_m^\beta | \pm \rangle = \sum_{s=0}^{2R-1} \text{pf} \mathcal{P}_{2R}^s. \quad (14)$$

with the pfaffian $\text{pf} \mathcal{P}_{2R}^s$ defined as in appendix A, Eq.(A1), where the entries of the $s - th$ column are replaced by zeros and the entries of the $s - th$ row are to be replaced by

$$\langle 0 | A_l B_m | 0 \rangle \longrightarrow \langle A_l B_m \rangle^{(\pm)}$$

with

$$\langle A_l B_m \rangle^{(\pm)} \doteq \langle \pm | A_l | 0 \rangle \langle 0 | B_m | \pm \rangle - \langle \pm | B_m | 0 \rangle \langle 0 | A_l | \pm \rangle.$$

Differently from the case where the average is performed over an equilibrium state, the correlators $\langle A_l A_m \rangle, \langle B_l B_m \rangle$ do not vanish. The relevant correlation functions to be computed are then (see [36] for details)

$$\begin{aligned} \langle A_l(t)B_m(t) \rangle^{(\pm)} = & - [V(i-m) \pm V(j-m)] [V(i-l) \pm V(j-l)] \\ & + [U^o(i-l) + U^e(i-l) \pm (U^o(j-l) + U^e(j-l))] \times \\ & [U^o(i-m) - U^e(i-m) \pm (U^o(j-m) - U^e(j-m))] \end{aligned} \quad (15)$$

$$\begin{aligned} \langle A_l(t)A_m(t) \rangle^{(\pm)} = & i \{ [V(i-m) \pm V(j-m)] [U^o(i-l) + U^e(i-l) \pm (U^o(j-l) + U^e(j-l))] \\ & - [V(i-l) \pm V(j-l)] [U^o(i-m) + U^e(i-m) \pm (U^o(j-m) + U^e(j-m))] \} \end{aligned} \quad (16)$$

$$\begin{aligned} \langle B_l(t)B_{l+R}(t) \rangle^{(\pm)} = & i \{ [V(i-m) \pm V(j-m)] [U^o(i-l) - U^e(i-l) \pm (U^o(j-l) - U^e(j-l))] \\ & - [V(i-l) \pm V(j-l)] [U^o(i-m) - U^e(i-m) \pm (U^o(j-m) - U^e(j-m))] \} , \end{aligned} \quad (17)$$

where

$$U^o(r) := \frac{\lambda\gamma}{\pi} \int_0^\pi k \sin k \frac{\sin(\Lambda_k t)}{\Lambda_k} \sin kr \quad (18)$$

$$U^e(r) := \frac{1}{\pi} \int_0^\pi k (1 + \lambda \cos k) \frac{\sin(\Lambda_k t)}{\Lambda_k} \cos kr \quad (19)$$

$$V(r) := \frac{1}{\pi} \int_0^\pi k \cos(\Lambda_k t) \cos kr \quad (20)$$

These two-point functions together with Eq.(14) allow to evaluate all the spin-correlation functions necessary for the calculation of the two-body reduced density matrix. Inaccessible by the above technique is the correlation $\langle \pm | S_l^x | \pm \rangle$. However, if $\langle \pm | S_l^{x,y}(t=0) | \pm \rangle = 0$, then it will remain zero during the subsequent evolution. This correlation is zero if the parity symmetry of the Hamiltonian is not broken by the initial and final state. We will consider exclusively this case in the present work.

In the case $\gamma = 0$ the particle number conservation leads to a considerable simplification since the vacuum is an eigenstate. For the XY-model we consider with some detail the case of the propagation of a singlet. In this case, because of the conservation of the total magnetization, only states with one reversed spin will enter the dynamics. In terms of corresponding fermions only one particle states are involved in the dynamics. Correlation functions can be evaluated directly without resorting to the techniques described above.

III. MEASURES OF ENTANGLEMENT

On a qualitative basis entanglement is well understood. Both for distinguishable particles (e.g. spins on a lattice) and identical particles (e.g. free fermions/bosons) it is known that if the wavefunction can be written as a (tensor-) product state and as the (anti-) symmetrization of such product states, respectively, then the corresponding degrees of freedom are not entangled [37]. In order to analyze entanglement properties of spin chains, we need to characterize entanglement at a quantitative level and therefore we have to use some measure for the entanglement stored in the chain. In general this is a formidable

task and it is not yet known how to completely accomplish it in a many-body system. As it was done in Refs. [15,16,18,19] we will consider here the entanglement of formation as a measure of entanglement. We confine our attention to the analysis of the entanglement of a given subsystem with the rest of the chain and to the entanglement between two arbitrary sites in the chain (for simplicity we will refer to such quantities as the amount entanglement). In the former case, accessible entanglement measures have been found when the total system is in a pure state. In the latter, i.e. for two-qubit entanglement, a measure is known also for the total system being in a mixed state.

A. Entanglement of a subsystem with its complement

In order to identify whether a pure state of the total system S is a product state of a part A and the rest of the system $B = S \setminus A$ it is sufficient to trace out A or B ; only in case of a product state, the rank of the outgoing reduced density matrix will be one. If the rank is larger than one, then we know that A and B are entangled. [37] A measure for the entanglement between these two subsystems is $S[\rho_A] := -\text{tr} \rho_A \log_{\dim A} \rho_A$, which is the von Neumann entropy of the subsystem A . $\dim A$ is the dimension of the Hilbert space corresponding to A and bounds the quantity to the interval $[0, 1]$. We analyze the case when the subsystem A is one site and the corresponding entanglement measure quantifies the entanglement of one site with the rest of the chain [38]

$$S[\rho^{(1)}] := -\text{tr} \rho^{(1)} \log_2 \rho^{(1)}$$

where $\rho_A = \rho_j^{(1)}$ is the one-site reduced density matrix. In this case, if there is no broken symmetry, this parameter is related to the average magnetization along the z component

$$\rho_j^{(1)} = \begin{pmatrix} \frac{1}{2} + \langle S_j^z \rangle & 0 \\ 0 & \frac{1}{2} - \langle S_j^z \rangle \end{pmatrix} \quad (21)$$

The one-site density matrix contains only one real unitarily invariant parameter: its eigenvalue $p \leq 1/2$. One can then choose other measures of the entanglement which are related to the von Neumann entropy. A relevant example is the (one-)tangle [29], whose importance stems from the fact that it was proved to be an additive measure of entanglement, including the two- and three-tangle for pure states of up to three qubits and there is some evidence for additivity also for larger ensembles. We will therefore in particular study the tangle in this work and will find further evidence for this surmised additivity formulated in Ref. [29]. The one-tangle is given by

$$\tau^{(1)}[\rho^{(1)}] := 4\det\rho^{(1)}$$

and is connected to the von Neumann entropy through the relation

$$S[\rho^{(1)}] = h\left(\frac{1}{2}\left(1 + \sqrt{1 - \tau_1[\rho^{(1)}]}\right)\right).$$

where $h(x) =: -x \log_2 x - (1-x) \log_2(1-x)$ [39]. Quantified by the tangle, the entanglement of the site j with the rest of the chain for the anisotropic transverse XY models is given by

$$\tau^{(1)}[\rho_j^{(1)}] = 4 \det \rho_1^{(j)} = \frac{1}{4} - \langle S_j^z \rangle^2. \quad (22)$$

For what follows we omit the index of the one-tangle and write $\tau := \tau^{(1)}$.

It must be stressed that the entanglement measures discussed so far are applicable only if the total system is found in a pure state; being in a mixed state one had to consider instead the minimum average of the above quantities evaluated on all possible decompositions of the density matrix of the total system. Without this minimization procedure an upper bound for the entanglement

is obtained, since the entanglement is a convex function in the space of density matrices [40,41].

B. Entanglement between two sites - Concurrence

All the information needed to analyze bipartite entanglement is contained in the two-qubit reduced density matrix $\rho^{(2)}$, obtained from the wave-function of the state after all the spins except those at positions i and j have been traced out. The resulting $\rho^{(2)}$ represents a mixed state of a bipartite system for which a good deal of work has been devoted to quantify its entanglement [42]. As a measure for arbitrary mixed states of two qubits, we use the concurrence [40] $C[\rho^{(2)}]$

$$C[\rho^{(2)}] := \max\{0, 2\lambda_{max} - \text{tr}\sqrt{R}\}, \quad (23)$$

$$R := \rho^{(2)}\sigma_y \otimes \sigma_y \rho^{(2)*} \sigma_y \otimes \sigma_y \quad (24)$$

where λ_{max} is the largest eigenvalue of the matrix \sqrt{R} , which is the product of $\rho^{(2)}$ with its time-reversed; σ_y is a Pauli matrix. For pure two-qubit states it is $\tau^{(1)} \equiv C^2 =: \tau^{(2)}$. The great advantage of the concurrence is that it is directly defined in terms of the density matrix $\rho^{(2)}$ without any minimization procedure; therefore it can be calculated from correlation functions of the corresponding Hamiltonian.

We derive the structure of the two-qubit reduced density matrix $\rho^{(2)}$ for the model Hamiltonian of Eq.(1). Certain symmetries of the Hamiltonian do restrict the structure of the reduced density matrix as long as they are not broken.

As discussed more in detail in Appendix B, the concurrence can be expressed in terms of spin correlation functions (see Eqs.(B4))

$$C_{lm} = 2 \max \left\{ 0, \sqrt{(g_{lm}^{xx} - g_{lm}^{yy})^2 + (g_{lm}^{xy} + g_{lm}^{yx})^2} - \sqrt{\left(\frac{1}{4} - g_{lm}^{zz}\right)^2 - \frac{1}{4}(M_l^z - M_m^z)^2}, \right. \\ \left. \sqrt{(g_{lm}^{xx} + g_{lm}^{yy})^2 + (g_{lm}^{xy} - g_{lm}^{yx})^2} - \sqrt{\left(\frac{1}{4} + g_{lm}^{zz}\right)^2 - \frac{1}{4}(M_l^z + M_m^z)^2} \right\}. \quad (25)$$

In the isotropic case ($\gamma = 0$) the conservation of magnetization, or equivalently of the total number of particles, the structure of the 2-site reduced density matrix simplifies considerably (provided that the initial state belongs to a definite spin sector of the overall Hilbert space). In this case the concurrence is given by

$$C^{iso} = \max \left\{ 0, 4|g_{lm}^{xx}| - \sqrt{\left(\frac{1 + 4g_{lm}^{zz}}{2}\right)^2 - 1(M_l^z + M_m^z)^2} \right\}. \quad (26)$$

As we will study the time evolution of a singlet (one of the Bell states) on top of the vacuum, the structure

of $\rho^{(2)}$ further simplifies because one has to deal with one-particle states only. This leads to a concurrence

$$C_{singlet}^{iso} = 4|g_{lm}^{xx}|. \quad (27)$$

C. The conjecture by Coffman, Kundu, and Wootters

One- and two- site entanglement do not furnish a complete characterization of the entanglement present in spin chains. In this direction it is interesting to study a conjecture put forward by Coffman, Kundu, and Wootters

that states that the sum of the two-tangles (the square of the concurrences) be at most equal to the one-tangle.

$$\sum_{j \neq n} C_{n,j}^2 \leq 4 \det \rho_n^{(1)} = \tau_n^{(1)}. \quad (28)$$

A non-zero difference in the above inequality has been interpreted as “residual tangle”, i.e. entanglement not stored in two-qubit entanglement. This inequality was proved in Ref. [29] for a three qubit system, giving rise to the definition of the three-tangle as a measure of three-qubit entanglement.

IV. RESULTS

A. $\gamma = 0$: The isotropic model

In this section, we describe the dynamics of entanglement for $\gamma = 0$. The Hamiltonian of Eq.(1) is then reduced to the XY model. We will discuss the case in which the initial condition is given by one of the maximally entangled Bell states as defined in Eq.(13), where the description of the entanglement dynamics is amenable to a quite simple analytical solution. Already for this case we will get many results that will emerge also in the analysis of the models for generic γ . As already mentioned, the feature that distinguishes this model from the general case is that the z -component of the total spin, S^z , is conserved. Consequently the Jordan-Wigner transformed fermionic Hamiltonian becomes a tight binding model for each sector with fixed S^z . The dynamics cannot generate entanglement from the vacuum state $|\downarrow\rangle = |\downarrow\rangle^{\otimes N}$ (as it turns out to occur for $\gamma \neq 0$).

We first consider the case of a chain initially prepared in a maximally entangled singlet-like state $|\Psi_{i,j}^\varphi\rangle$ on sites i and j as defined in Eq. (13). By using the evolution of the fermion operators obtained in Eq.(9), the state vector at later times is found to be

$$|\Psi_{i,j}^\varphi\rangle = \sum_l w_l(t) c_l^\dagger |\downarrow\rangle \quad (29)$$

with

$$w_l(t) = \frac{1}{\sqrt{2N}} \sum_k \left[e^{\frac{2\pi ik}{N}(i-l)} + e^{i\varphi} e^{\frac{2\pi ik}{N}(j-l)} \right] e^{i\Lambda_k t}. \quad (30)$$

In the thermodynamic limit, $N \rightarrow \infty$, the coefficients become

$$w_l(t) = \frac{1}{\sqrt{2}} \left\{ J_{i-l}(\lambda t) + e^{i\varphi} (-i)^{(j-i)} J_{j-l}(\lambda t) \right\}, \quad (31)$$

where $J_n(x)$ is the Bessel function of order n (we omitted an irrelevant global time dependent phase).

1. Concurrence

For the initial singlet-like state of Eq.(29), it can be shown that the concurrence between two selected sites n and m is given by

$$C_{n,m}(t) = 2 \left| w_n(t) w_m^*(t) \right|. \quad (32)$$

This expression is plotted in Figs. 1–4 for some particular cases.

The time evolution dictated by the Hamiltonian, amounts to a simultaneous spin flip between sites l and $l \pm 1$, i.e.: a propagation of the single flipped spin in either directions. Expressed in terms of the fermion operators the Hamiltonian becomes a tight-binding model. In particular, this implies that each one of the initially entangled sites (say i) tends to become entangled with the nearest neighbors of the other ($j \pm 1$). The time scale is set up by the interaction strength, so that the information exchange or “entanglement propagation” over a distance of d lattice spacings, approximately takes a time $t \sim d/\lambda$. The external local field h does not enter anyway, due to the fact that all of the components of the state (29) are in the same spin sector of the Hilbert space.

The concurrence defined in Eq.(32) depends on four sites: apart from n and m , whose entanglement we want to measure, also the initially entangled ones, i and j , enter the general expression for $C_{n,m}$. We first look at the decay of the concurrence shared by the initially maximally entangled sites themselves depending on their distance x (i.e. $j = i + x$). The result is seen in Fig. 1.

$$C_{i,i+x} = \left| J_0^2 + 2i^x J_0 J_x \cos \varphi + (-1)^x J_x^2 \right|, \quad (33)$$

where the Bessel functions J have to be evaluated at λt . After a first recurrence of the entanglement at the time $t \sim x/\lambda$ (due to the swap between the two sites), the concurrence decays at longer times as t^{-1} , modulated by the subsequent revivals of the entanglement at times which are integer multiples of the first revival time, and by oscillations of period λ^{-1} .

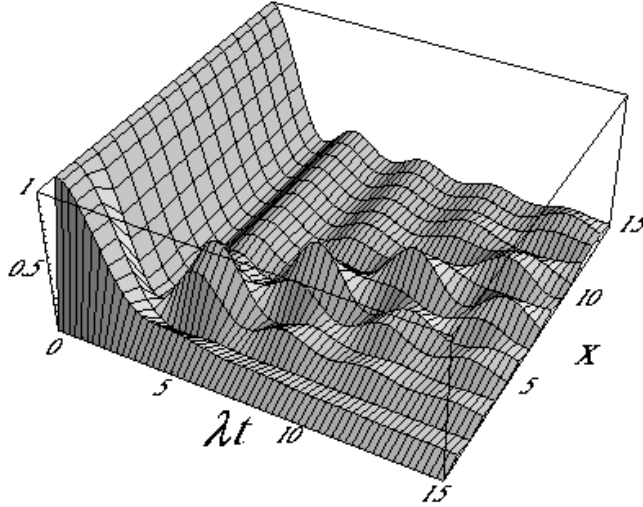


FIG. 1. Concurrence $C_{i,i+x}$ as a function of time and of the distance between the initially entangled sites. The initial state is a singlet ($\varphi = \pi$ in the initial condition) involving the very same sites i and $i+x$.

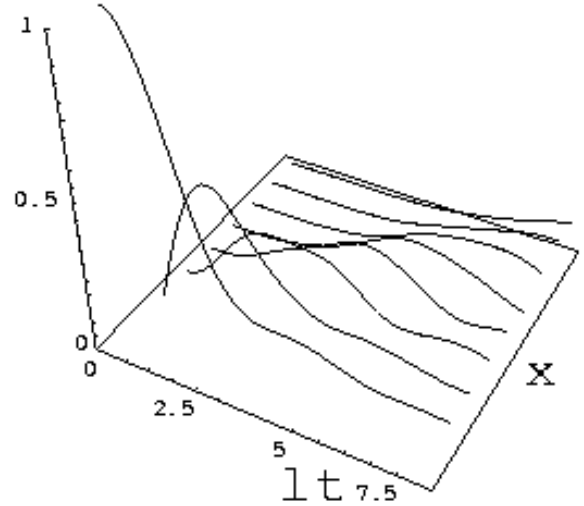


FIG. 2. Concurrence between sites at a distance x (namely, $n = i$, and $n = i+x$ in Eq. 32), for the case of an initial 0-triplet state ($\varphi = 0$) shared by two nearest neighbor sites, $i = 0, j = 1$. The various plots correspond to $x = 1, \dots, 8$.

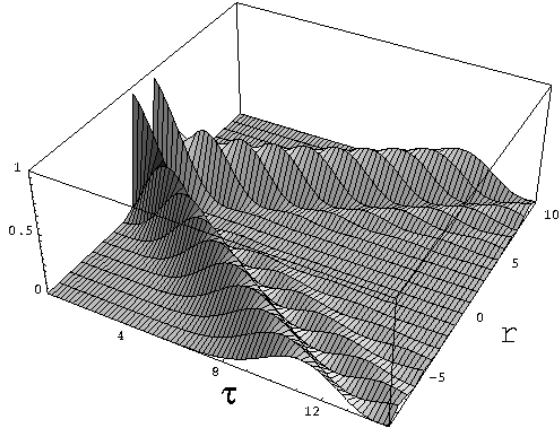


FIG. 3. Concurrence between sites $n = -x, m = x$, symmetrically displaced from their initial position $i = -1$ and $j = 1$ ($\varphi = \pi$).

We now concentrate on the distribution and propagation of the entanglement. Supposing that the initially selected sites are nearest neighbors, $j = i + 1$, we look at the concurrence between one of these two (namely, i) and another site of the chain at distance x (i.e. $n = i$ and $m = i+x$ in Eq.(32)). The result is shown in Fig.2, where one can see the propagation of the maximum with velocity λ . As already pointed out, the dynamics of the model consists in flipping the spin of neighbor sites, leading to a propagation of the initially flipped spin along the chain both in the same and in opposite directions. This comprises a propagation of the concurrence as confirmed by Fig.3, where the concurrence is shown between two sites symmetrically displaced with respect to the initial

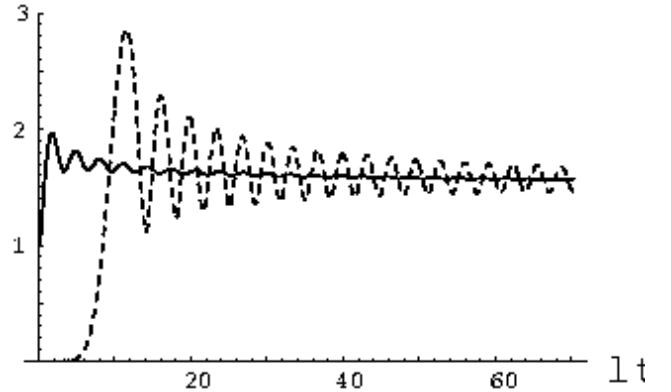


FIG. 4. Summed concurrences for an initially entangled site ($n = 0$, full line) and an initially unentangled site ($n = 10$, dashed line). The initial state is a singlet ($\varphi = \pi$) created on sites $i = 0$ and $j = 1$.

excitation (namely, $i = -1$ and $j = 1$ as initially entangled pair of sites, and $n = x, m = -x$ in Eq. (32)). This can be regarded as the propagation of an EPR-like pair; also in this case the speed of propagation is λ . In Fig.4, the total concurrence

$$C_{tot,n} = \sum_m C_{n,m}$$

of the single site n is shown, representing the total amount of pairwise entanglement involving the selected site. We found that the same stationary value (around 1.6) is reached for all values of n , independently of the initial conditions. This demonstrates that the initial state becomes homogeneously spread at long times and so does the concurrence.

2. Entropy

For a deeper investigation of the entanglement propagation observed for the concurrence $C_{n,m}$, we evaluate the entropy $S_{n,m}^{(2)}$ of the reduced density matrix $\rho_{n,m}^{(2)}$. Since the chain is in a pure state, this entropy gives a measure of the entanglement of the two sites with the rest of the chain. In particular, if $S_{n,m}^{(2)} = 0$, then the state of the two sites is pure and no entanglement exists with the rest of the chain, while $S_{n,m}^{(2)} \neq 0$ means that $\rho_{n,m}^{(2)}$ is a mixed state, and consequently the pair (n, m) is entangled with the rest of the system.

From the two-site reduced density matrix for this case, Eq. (B13) in the Appendix, we deduce

$$S_{n,m}^{(2)}(t) = -(1-p)\log_2(1-p) - p\log_2 p, \quad (34)$$

with $p = |w_n(t)|^2 + |w_m(t)|^2$. $S_{-x,x+1}^{(2)}$ is shown in Fig. 5 unveiling the same qualitative structure found for the concurrence. In particular, the propagation velocity is the same. Initially, this entropy is zero and for $x > 0$ it remains zero until the “entanglement wave” has arrived. This is because a pure state $|\downarrow\rangle_n |\downarrow\rangle_m$ is found before. Then the pair of spins becomes entangled not only between themselves, but also with the rest of the system. This is understood in the sense of entanglement sharing [29] from the fact that also the nearest neighbors x and $x+1$ become entangled at that time. After that, the two sites are left partially entangled with the rest of the chain.

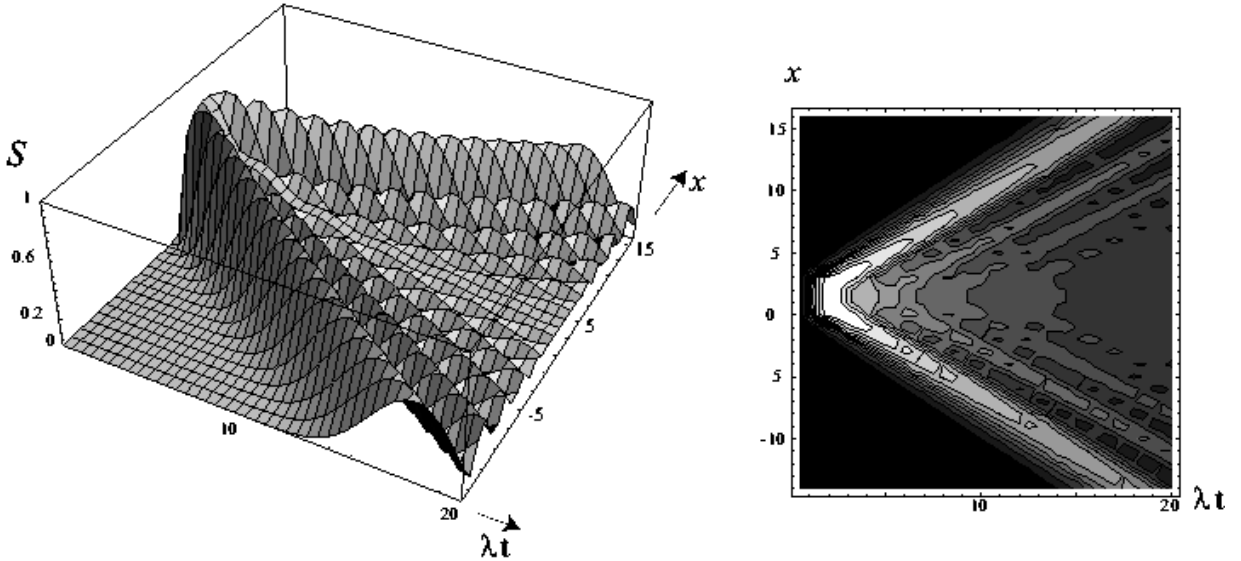


FIG. 5. Entropy $S_{(-x,x+1)}^{(2)}(\tau)$ for pairs of sites symmetrically displaced with respect to the initial singlet position at $(i, j) = (0, 1)$. This is for $\varphi = \pi$.

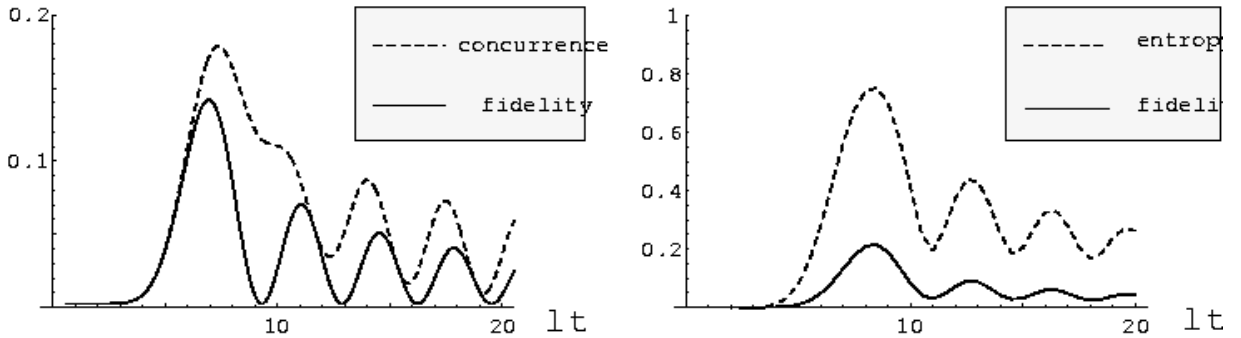


FIG. 6. Comparison between the temporal behaviors of the fidelity and the concurrence (left) or entropy (right), for the cases $(a, b) = (-1, 1)$, $(n, m) = (-6, 6)$ for $\varphi = \pi/2$ (left) and $(a, b) = (0, 1)$, $(n, m) = (-6, 7)$ for $\varphi = \pi$ (right).

The above discussion can be extended to the von Neumann entropy for an N -site subsystem at positions $\vec{j} := (j_1, \dots, j_N)$: since the reduced density matrix has still rank 2 we still have $S_j^{(N)} = -p \log_2 p - (1-p) \log_2 1-p$ but with $p = \sum_{i=1}^N |w_{j_i}|^2$. This gives access to the time dependence of the entropy also for a block of spins in the system. Such a quantity was studied at equilibrium in Ref. [20].

3. One-site entanglement and the CKW conjecture

The same structure as for the two-site entropy is also found in the single site entropy, $S_n^{(1)}(t)$, quantifying the amount of entanglement of one site with all the other spins (see Fig. 7). Also this can be understood from the CKW conjecture [29] as explained in what follows.

For the isotropic model it is possible to analytically check this conjecture. All needed quantities are known explicitly and we obtain

$$4 \det \rho_j^{(1)} = 4|w_j|^2(1 - |w_j|^2)$$

and

$$\sum_{n \neq j} C_{j,n}^2 = 4 \sum_{n \neq j} |w_j w_n^*|^2 = 4|w_j|^2(1 - |w_j|^2).$$

Thus, the two quantities coincide, meaning that the entanglement present in the system is restricted to the class of pairwise entanglement, and no higher order entanglement is created. Since, as mentioned in the previous section, the one-tangle is a monotonic function of the von Neumann entropy, the information gained from studying the entropies of the system is already (implicitly) contained in the concurrence. This has already been observed for these Werner-type states in Ref. [29].

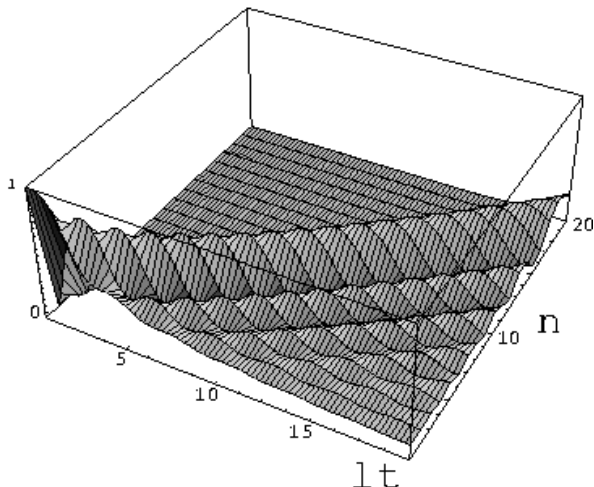


FIG. 7. Entanglement of the site n with the rest of the chain quantified by the entropy of the one-site reduced density matrix. The initial state was a singlet at $(a, b) = (0, 1)$.

4. Fidelity

In order to gain information on what type of Bell state propagates and on eventual state mutation, we study how similar is the mixed state $\rho_{n,m}^{(2)}$ to the initial $|\Psi^\varphi\rangle$ [43]. This similarity is quantified by the fidelity

$$F_{n,m}(t) = \text{Tr} \left\{ \rho_{n,m}^{(2)}(t) |\Psi^\varphi\rangle \langle \Psi^\varphi| \right\}, \quad (35)$$

which is found to be

$$F_{n,m}(t) = \frac{1}{2} |w_n(t) + e^{-i\varphi} w_m(t)|^2. \quad (36)$$

We compare this quantity to both concurrence and entropy in Fig. 6, where it is shown that the fidelity displays in-phase oscillation with respect to both the entanglement measures. Thus, when the entanglement wave arrives, $\rho_{n,m}^{(2)}$ becomes more similar to the initially prepared state. We can interpret this by saying that the state itself is propagating along the chain, although this propagation is far from a perfect transmission, due to the entanglement sharing with many sites at a time.

B. Other maximally entangled states

Apart from the states $|\Psi^\varphi\rangle$ of Eq. (13), we also analyzed the propagation of entanglement starting from other maximally entangled states, of the form

$$\begin{aligned} |\Phi_{i,j}^\varphi\rangle &= \frac{1}{\sqrt{2}} (|\downarrow_i, \downarrow_j\rangle + e^{i\varphi} |\uparrow_i, \uparrow_j\rangle) \otimes |\downarrow\rangle^{\otimes(N-2)} \\ &= \frac{1}{\sqrt{2}} (\mathbf{1} + e^{i\varphi} c_i^\dagger c_j^\dagger) |\downarrow\rangle. \end{aligned} \quad (37)$$

These are not single-particle states and, furthermore, since they are superpositions of two components pertaining to different spin sectors of the global Hilbert space, one cannot take full advantage of the conservation of the magnetization. As a result, the two-site reduced density matrix for this case is of the form of Eq. (B1), and the concurrence is given by $C = \max\{0, C^{(1)}, C^{(2)}\}$ (see Eq. (B2)); a concurrence of the form $C^{(2)}$ indicates that $|\Psi\rangle$ -like correlation arises, while for $C^{(1)} > C^{(2)}$ the correlations between the two selected sites is more $|\Phi\rangle$ -like.

As we will show, the entanglement propagates with velocity λ along the chain also for the initial condition (37). Under certain conditions, however, a clear difference arises with respect to the situation analyzed in the previous section; namely, when the two initially entangled sites are separated by an odd number of spins. It turns out that then, the propagating quantum correlations change their character after a while, and from that point on a singlet-like concurrence continues propagating

even if the initial state was not a singlet. To demonstrate this, we study the time evolution of an initial Bell state $|\Phi_{i,j}^\varphi\rangle$ and the fidelity of the Bell states $|\Phi_{m,n}^{\varphi'}\rangle$ and $|\Psi_{m,n}^{\varphi'}\rangle$ in the actual two-site states.

The time evolution of the various coefficients involved in the evaluation of C can be obtained using once again Eq. (9). In the thermodynamic limit ($N \rightarrow \infty$) and by looking at the sites n, m (with $m > n$, for definiteness), we find

$$a = \frac{1}{2} [J_{n-i}J_{m-j} - J_{n-j}J_{m-i}]^2, \quad (38)$$

$$b = 1 + a - \frac{1}{2} [J_{m-i}^2 + J_{n-i}^2 + J_{m-j}^2 + J_{n-j}^2], \quad (39)$$

$$|c| = \frac{1}{2} |J_{n-i}J_{m-j} - J_{m-i}J_{n-j}| \quad (40)$$

$$x = \frac{1}{2} [J_{n-i}^2 + J_{n-j}^2] - a, \quad (41)$$

$$y = \frac{1}{2} [J_{m-i}^2 + J_{m-j}^2] - a, \quad (42)$$

$$|z| = \left| \frac{1}{2} (J_{m-i}J_{n-i} + J_{m-j}J_{n-j}) - \sum_{r=n+1}^{m-1} (J_{n-i}J_{r-j} - J_{n-j}J_{r-i}) (J_{m-i}J_{r-j} - J_{m-j}J_{r-i}) \right|, \quad (43)$$

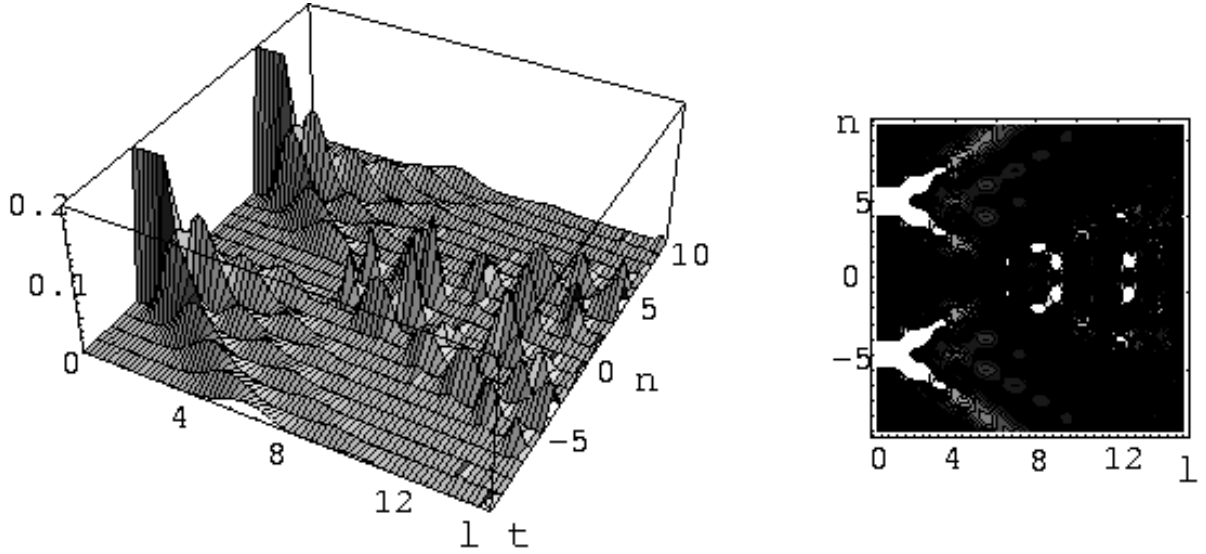


FIG. 8. Time evolution of the concurrence between sites $-n$ and n for the initial state $|\Phi_{-5,5}^\varphi\rangle$. The plot is cut at 0.2 in order to make the revival after the crossing visible.

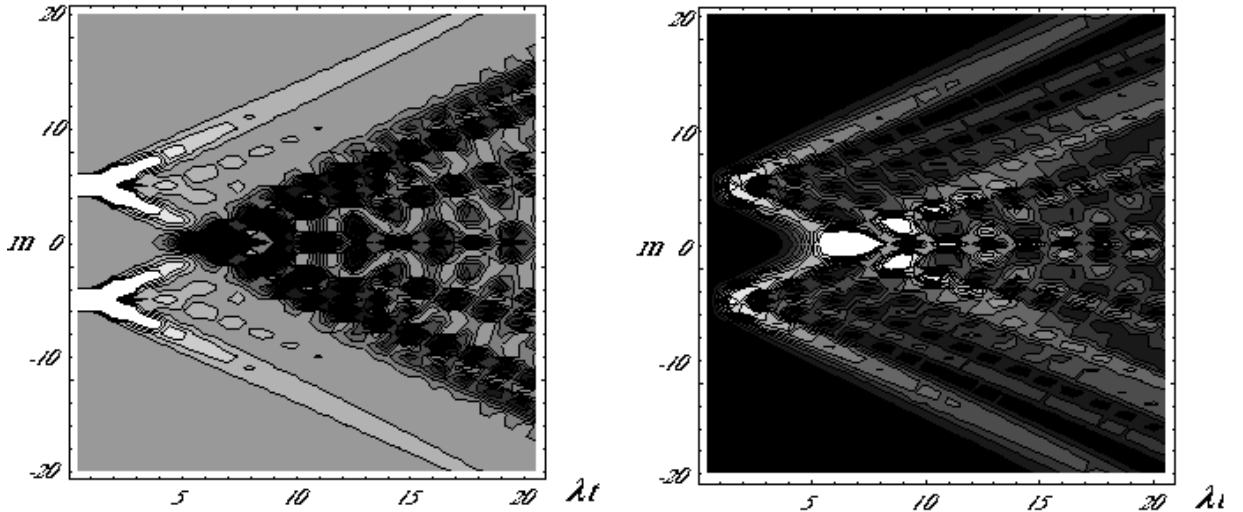


FIG. 9. Degree of similarity (white:high, black:low) between the density matrix $\rho_{-n,n}^{(2)}(t)$ and the states $|\Phi^{\varphi_{opt}}\rangle$ (left) and $|\Psi^{\varphi_{opt}}\rangle$ (right) (quantified by the corresponding fidelities).

where all the Bessel functions are evaluated at λt . We note that any dependence on the phase φ of the initial superposition has disappeared (only the phase of c depends on φ).

The concurrence is then readily obtained from these expressions. An example is shown in Fig. (8), where $C_{-n,n}$ is displayed for an initial state $|\Phi_{-5,5}^\varphi\rangle$. One can see that the concurrence between the original Bell state positions suddenly decays while the maximum propagates along the chain. At the intersection between the two peaks coming from the initial Bell state, however, a

revival is present. From this time on, the entanglement spreads out from this middle point. A detailed analysis reveals that at the crossing the concurrence switches from $C^{(1)}$ to $C^{(2)}$. This indicates that quantum correlations of type $|\Phi\rangle$ do not propagate much along the chain before changing to singlet-like correlations (of type $|\Psi\rangle$) in this case. In order to make visible this switching from the initial triplet to a singlet-like state, we analyzed the degree of resemblance of the two-site density matrix with both the states $|\Phi^{\varphi'}\rangle$ and $|\Psi^{\varphi'}\rangle$. These two fidelities are given by

$$\text{Tr} \left\{ \rho_{n,m}^{(2)}(t) \left| \Phi^{\varphi'} \right\rangle \left\langle \Phi^{\varphi'} \right| \right\} = \frac{a+b}{2} + |c| \cos \left[(\varphi' - \varphi) + \frac{\pi}{2}(m+n-i-j) \right] \quad (44)$$

$$\text{Tr} \left\{ \rho_{n,m}^{(2)}(t) \left| \Psi^{\varphi'} \right\rangle \left\langle \Psi^{\varphi'} \right| \right\} = \frac{x+y}{2} + |z| \cos \left[\varphi' + \frac{\pi}{2}(n-m) \right] \quad (45)$$

It can be seen from these relations that there exist “optimal” phases that maximize the two degrees of resemblance, namely

$$\varphi_{opt}^\Phi = \varphi + \frac{\pi}{2}(a+b-m-n), \quad \varphi_{opt}^\Psi = \frac{\pi}{2}(m-n),$$

respectively, which depend only on the positions along the chain (m and n) and on the initially excited sites (i and j) but do not depend on time. In Fig. (9), we show the fidelity of $|\Phi^{\varphi_{opt}}\rangle$ (left plot) and $|\Psi^{\varphi_{opt}}\rangle$ (right plot) in $\rho_{-m,m}^{(2)}(t)$. We used the same initial conditions as in the evaluation of the concurrence in Fig. (8). Taking into account that the degree of similarity with a state $|\Phi^\varphi\rangle$ is 0.5 before the arrival of the entanglement wave (due to its $|\downarrow, \downarrow\rangle$ component), it is seen from these plots that after the crossing point the state of the pair of sites becomes $|\Psi\rangle$ -like.

As stated above, this phenomenon of a $|\Phi\rangle$ -like state turning into a $|\Psi\rangle$ -like state during the propagation only occurs in certain cases, and in particular every time two “entanglement waves” coming from the two sides of the chain intersect on a given spin (the site 0 in the example above). At the crossing, the amplitude for two parallel spins does not survive and the outgoing states of this scattering event only contain antiparallel spins. On the contrary, when the initially entangled spins are separated by an even number of sites, the crossing involves two sites and the character of the state is preserved.

C. $\gamma \neq 0$: Singlet onto the vacuum

We now move to consider the case of generic γ for an infinitely long chain. In contrast to the previous section, where the isotropic model (i.e. $\gamma = 0$) was examined, here the complexity of the computation grows with the distance d of the sites because the dimension of the Pfaffian expression for the correlation functions is $2d \times 2d$.

Therefore we focus our investigation on $d \in \{1, 2, 3\}$. For the critical Ising model (i.e. $\gamma = \lambda = 1$) it turns out to be sufficient considering $d = 1$, since the concurrence for the larger distances vanishes.

The initial state (at time $t = 0$) is the singlet created at the sites with number 1 and 2 onto the vacuum $|\downarrow\rangle$: $|\Psi_{1,2}^\pi\rangle = 1/\sqrt{2}(|\uparrow\downarrow\rangle - |\downarrow\uparrow\rangle) \hat{=} 1/\sqrt{2}(c_1^\dagger - c_2^\dagger)|\downarrow\rangle$. We start from small nonzero γ , then going to medium anisotropy, $\gamma = 0.5$, toward the transverse Ising model, $\gamma = 1$. The initial state, as well as the Hamiltonian, is invariant under a reflection by a mirror placed between the sites 1 and 2 up to a global prefactor (which does not affect the concurrence). Because of this mirror symmetry, we only show the propagation in direction of increasing site number. The propagation to the other side is the mirror image as in the previous figures.

1. Concurrence

Figure 10 shows the nearest neighbor concurrence for $\gamma = 0.1, 0.5, 1.0$ (from the top to the bottom) and $\lambda = 0.5, 1.0$ (left and right, respectively). A rough estimate of the propagation velocity can be taken from the contour lines in the plot. For not too large γ we find concurrence propagation roughly with velocity λ as for the isotropic model. For increasing γ (see the right column – $\lambda = 1$ – of Fig. 10) it slightly increases. The concurrence on the original singlet position decays quickly and oscillations are increasingly damped.

We notice (Fig.10) an instantaneous signal which, sufficiently far away from the initial singlet position is spatially uniform. This phenomenon reflects the creation of entanglement from the vacuum, which is characteristic for the anisotropic XY models. It is originated from the double spin flip operators $\gamma\lambda/2 \sum_i s_i^+ s_{i+1}^+$ (and its Hermitean conjugate), which are absent in the isotropic

model. Estimating the effect of this operator to second order in λt we argue that it transforms the vacuum into an entangled state corresponding to the bell states $|\uparrow\uparrow\rangle \pm |\downarrow\downarrow\rangle$; the nearest neighbor concurrence, originated

from these terms only, turns out to be

$$C_{k,k+1} = \gamma\lambda t - \gamma^2\lambda^2 t^2/2 . \quad (46)$$

That is, a linear increase with slope $\lambda\gamma$ and maximum value $C_{k,k+1}^{max} = 0.5$ at $t_{max} = 1/\lambda\gamma$.

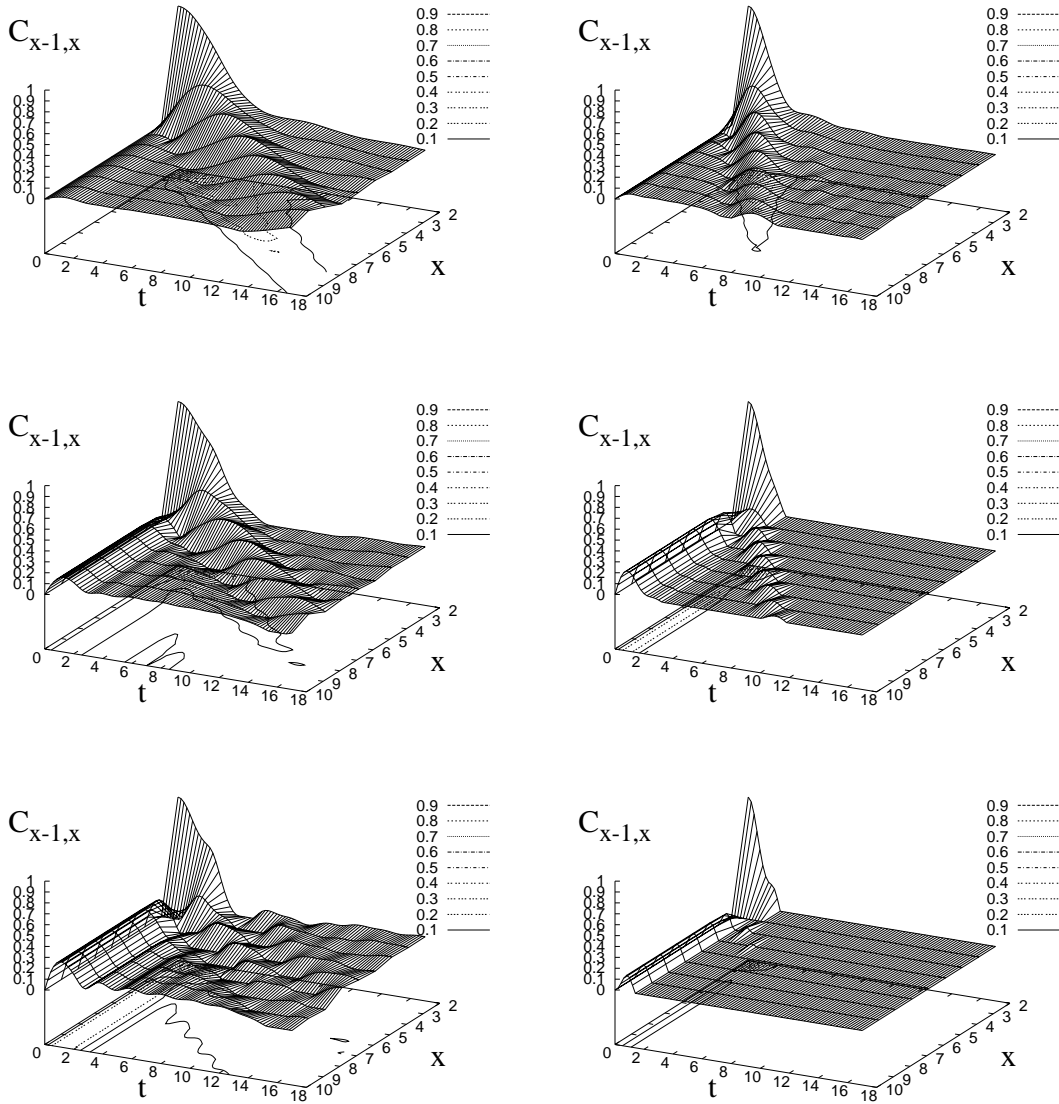


FIG. 10. *Top panel* - The nearest neighbor concurrence for the anisotropy $\gamma = 0.1$ and two different values of λ ($\lambda = 0.5$ left, $\lambda = 1$ right). As for the isotropic model, also here the singlet gets propagated roughly with velocity $v = \lambda$. There is a new feature, though, which is the small concurrence wall created from the vacuum. At the critical coupling $\lambda = 1$ the propagation is damped slightly stronger, but there are no drastic changes. *Middle panel* - The nearest neighbor concurrence for $\lambda = 0.5$ and medium anisotropy $\gamma = 0.5$; that is where the spin-wave approximation breaks down. Also here the singlet gets propagated roughly with velocity λ in proper units, but it is stronger damped than for $\gamma = 0.1$. The creation from the vacuum is instead sharply enhanced and survives at least until it reaches the propagating pulse. At the critical coupling, the nearest neighbor concurrence from the initial singlet dies out immediately and so does the vacuum creation. Only few bumps are indicating a glimpse of a propagation.

Whereas the initial slope of concurrence creation agrees with the exact calculation, the maximum differs significantly even for $\gamma = 1$, indicating that the kinetic term dispersively suppresses the concurrence evolving from the vacuum. In fact, the pure vacuum signal dies out very quickly. Towards the critical coupling and the Ising model, the damping of the concurrence propagation gets stronger. The vacuum signal survives much longer for medium λ and $\gamma \rightarrow 1$ such that for $\gamma = 0.5$ and $\gamma = 1$ it interferes with the propagating singlet. Although the damping of the propagation becomes stronger at the critical coupling, nevertheless it is of pure dynamic origin and not related to the quantum phase transition since, for generic γ , the energy of the vacuum is higher than the ground state energy (where the critical behaviour is encoded in). Consistently, the damping turned out to be independent of the size of the chain. [17,44]

For $\gamma = 0.1$ the most notable effect is the propagation of the singlet as for the isotropic model. The concurrence for this γ is shown in the mid pannel of Fig. 10: We still see a clear propagation of the concurrence, which is only slightly stronger damped than for the isotropic model, but the creation from the vacuum is much enhanced and

survives longer. A “shoulder” appears in the singlet peak of $C_{i,i+1}$, i.e. on the original singlet position. A better understanding of the evolution of the initial entangled state can be reached by evaluating the overlap of the reduced density matrix with the four Bell states. This is shown in Fig. 11) where the four plots refer to the fidelity to the corresponding Bell states indicated above. We see that the singlet-fidelity (shown in the upper leftmost picture in Fig. 11) does not have a shoulder, meaning that this feature is an effect associated to a formation of a triplet-type Bell state. In the plot of the fidelity for $\gamma = \lambda = 0.5$ (figure 11) we see that the main contribution to the propagation is coming from the singlet and the triplet $1/\sqrt{2}(|\uparrow\downarrow\rangle + |\downarrow\uparrow\rangle)$, which we call the 0-triplet. The initially predominant signal is the singlet; it seems though, that the singlet signal decays quicker than the 0-triplet. Hence could it be that after some time the singlet switched to the 0-triplet. Furthermore, we extract from the rightmost pictures of figure 11, showing the fidelities of the \pm -triplets $1/\sqrt{2}(|\uparrow\uparrow\rangle \pm |\downarrow\downarrow\rangle)$, that the entanglement created from the vacuum is of triplet type as estimated above (46).

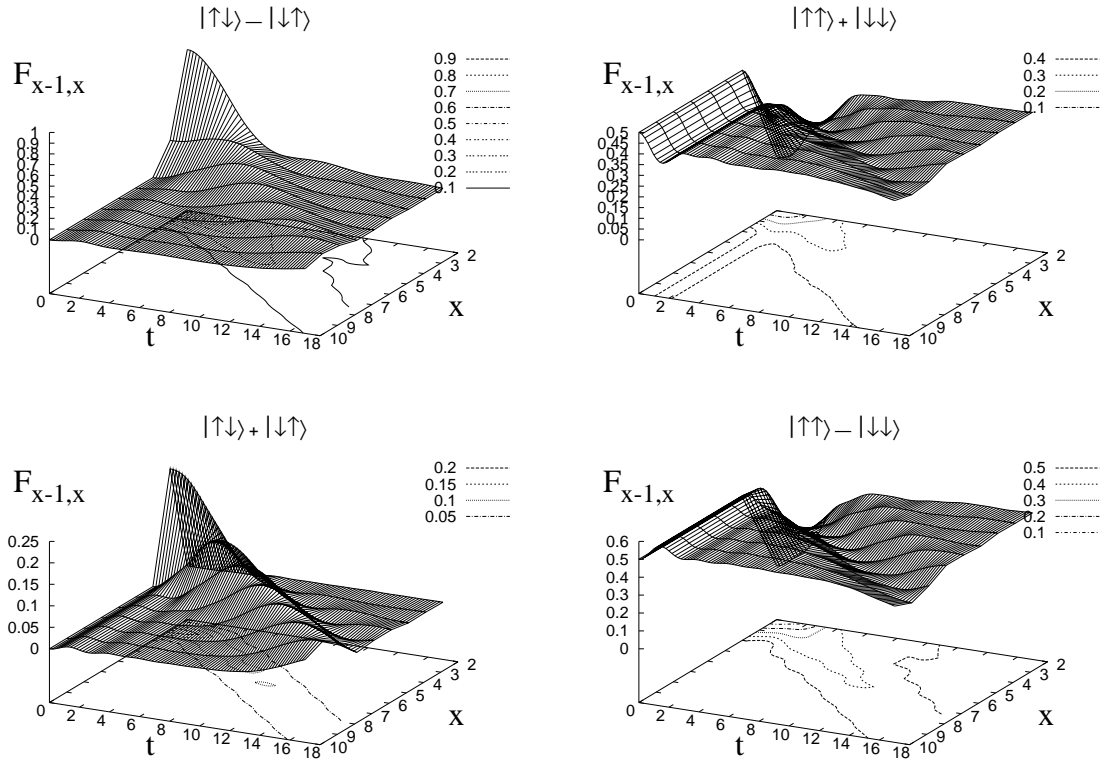


FIG. 11. The fidelity, here the portion of the four Bell states, i.e a singlet and three triplets, in the reduced density matrix is drawn for $\gamma = \lambda = 0.5$. Since an equal mixture of two Bell states is a disentangled state, the pictures show that the predominant Bell state in the propagation is indeed the singlet (upper leftmost picture), even though the triplet with zero S^z component (lower leftmost picture) decays slower and eventually could become dominant after sufficient time. It can also be seen that the vacuum creation is dominated by the Bell state antisymmetric under σ^x spin flip, i.e. $1/\sqrt{2}(|\uparrow\uparrow\rangle - |\downarrow\downarrow\rangle)$ (lower rightmost picture). In fact it grows on cost of its symmetric “brother”.

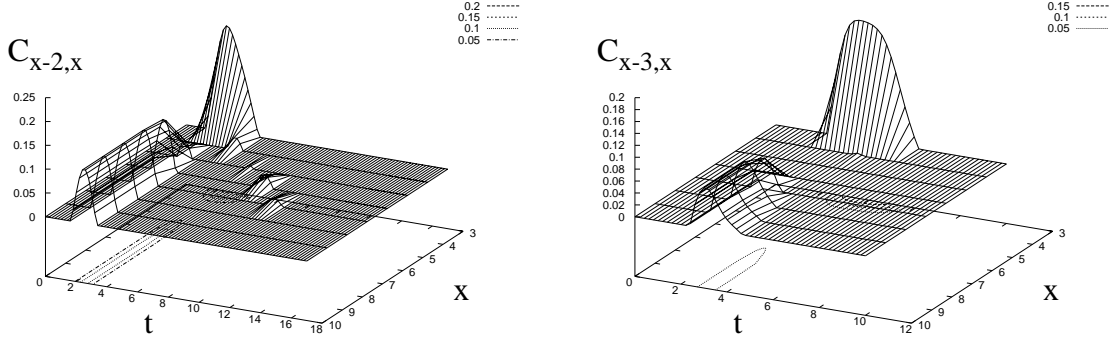


FIG. 12. *Left* - The next nearest neighbor concurrence C_2 for the Ising model far from the critical coupling. At the critical coupling it is zero. *Right* - The next next nearest neighbor concurrence C_3 for the Ising model far from the critical coupling. At the critical coupling, also C_3 vanishes. At $\lambda = 0.5$ we see a considerably large signal, which is due to an EPR-type propagation of a “split” singlet in the sense that the singlet somewhat splits up into two which separately propagate in opposite direction. Much as the two EPR photons originated from the relaxation of an s state of an atom at rest. The first EPR-signal is that one observed in this figure and corresponds to the concurrence between site 0 and 3, which are located one site to the left and right, respectively, of the original singlet sitting on sites 1 and 2. This concurrence propagation was also observed for the isotropic XY model and we expect that this signal should continue to larger distances, though stronger suppressed for generic γ . It is absent for the Ising model at the critical coupling.

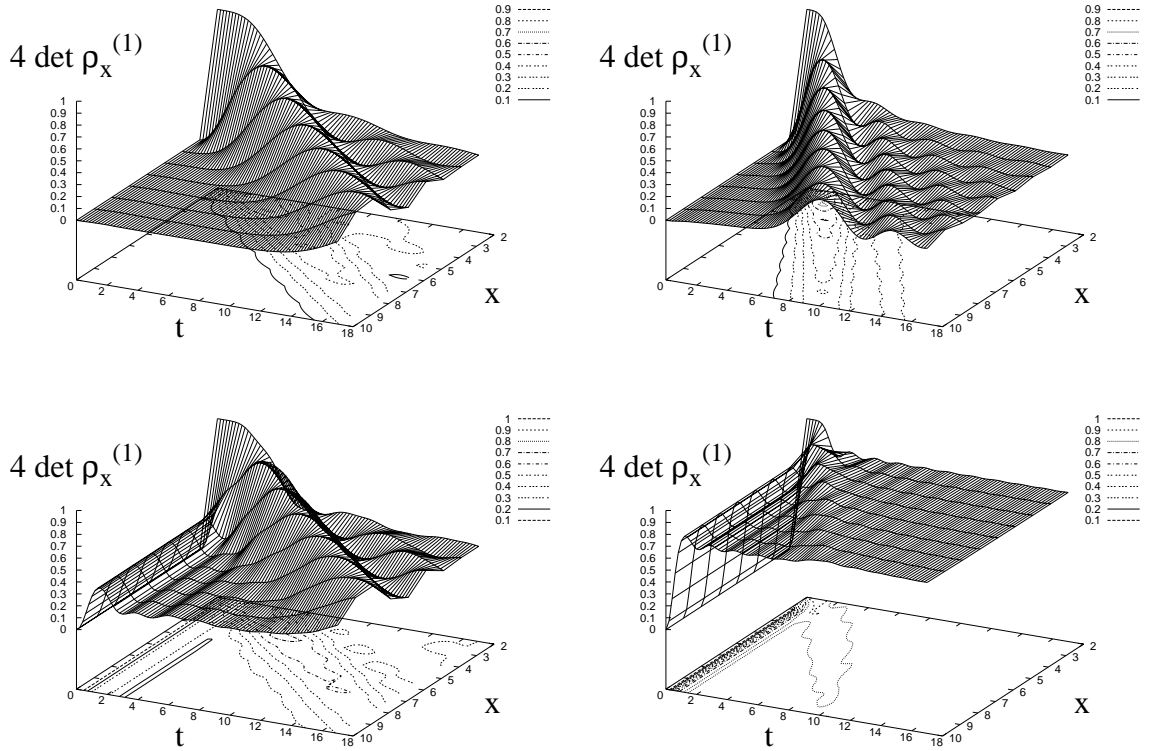


FIG. 13. The total tangle of site x *Upper panel* - for $\gamma = 0.1$. the plot qualitatively is very similar to the nearest neighbor concurrence squared; only the propagation is enhanced. This holds true for $\lambda = 0.5$ (left) and at critical coupling. *Lower panel* - for $\gamma = 1$. In contrast to the nearest neighbor concurrence there is a clear propagating signal here for $\lambda = 0.5$ (left). It is mounted on top of a non-zero background signal coming from the vacuum. At critical coupling the vacuum background of the one-tangle is grown up to about 0.75, whereas the propagation is hardly visible.

For the transverse Ising model, the shoulder on the original singlet position and the vacuum creation get even more pronounced, but all the signals die out much quicker. For $\lambda = 0.5$ one cannot speak any more of a clearly propagating entanglement signal (lower panel in Fig. 10). At the critical coupling, the propagating signal disappeared completely, small revivals of which can still be seen near the critical coupling. Whereas the features in the fidelity concerning the pulse propagation are essentially the same as described above for $\gamma = \lambda = 0.5$, it is interesting to note that at the critical coupling, all four fidelities seem to tend to a finite homogeneous value (without figure). The next-nearest neighbor and next-next-nearest neighbor concurrence is shown in Fig. 12. Both show a narrow wall created from the vacuum, which for $C_3 := C_{x-3,x}$ is broader. C_3 unveils an additional feature: it shows a large contribution at t around 4 at $x = 3$. It is caused by the original singlet kind of “split-

ting up” into two fragments, which independently propagate in opposite directions. As the singlet initially was positioned on the sites 1 and 2, these fragments after some time should be observed on sites 0 and 3, corresponding exactly to the peak observed in the figure 12. This phenomenon resembles an EPR-type propagation, which we observed already for the isotropic model (see Fig. 3). At the critical coupling C_2 and C_3 identically vanish on the domain of the demonstrated plots.

2. The global tangle

Is it possible to understand how the entanglement, originally stored into the singlet, is going to share among all the spins in the chain? In order to get an idea about what might happen, we study the one-site reduced density matrix ρ_1 .

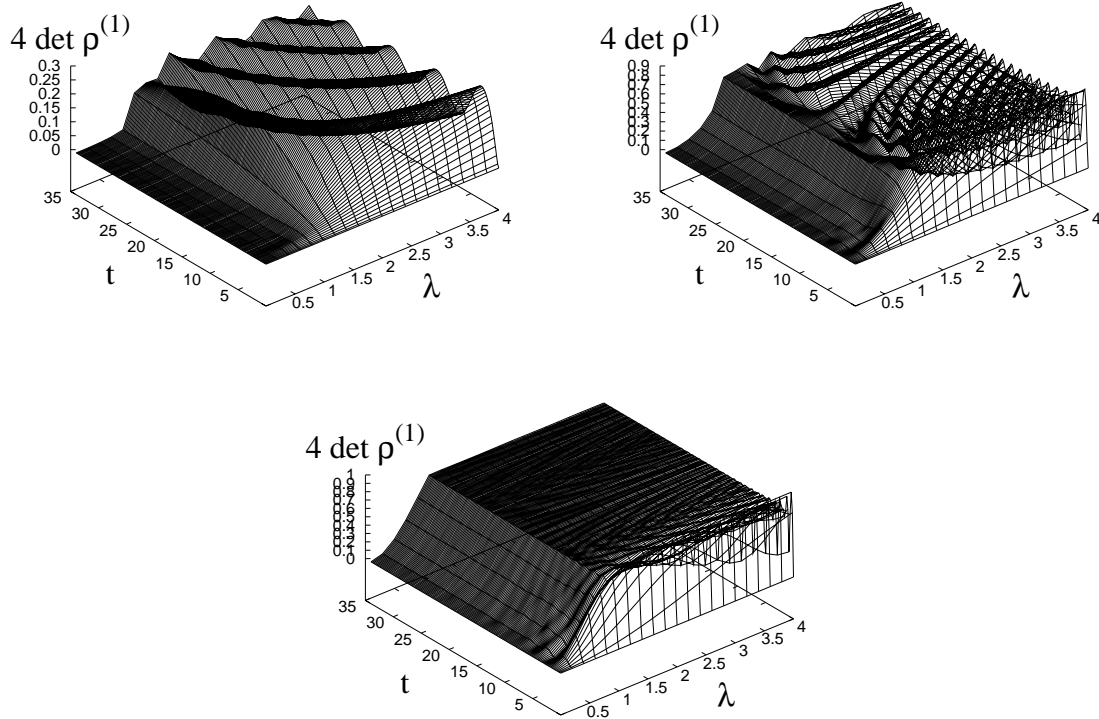


FIG. 14. The global tangle for the initial state being the vacuum and anisotropies $\gamma = 0.1, 0.5$, and 1 from left to the right. *left : small anisotropy.* For $\lambda < 1$ there is hardly any entanglement created by the Hamiltonian from the vacuum. This abruptly changes at the critical coupling $\lambda = 1$. The abruptness manifests itself in the large exponent in a rough polynomial fit up to $\lambda = 1$ at time $t = 17$, which here gives $0.1 \lambda^{8.2}$. For $\lambda > 1$ strong oscillations emerge with an amplitude of roughly 30% of the average value. About 10% oscillation amplitude is also present for $\lambda < 1$, though unresolved in the plot. *middle: medium anisotropy.* Here we observe a much more smooth increase of the average entanglement, when λ increases. The corresponding rough fit is $.55 \lambda^{3.3}$. As a function of time it very soon saturates. Only beyond the critical interaction strength there are oscillation around this value but with an amplitude of few percent of the average value. *right: quantum Ising model.* Towards the Ising model the saturation value of the tangle increases more and more quickly with λ . The polynomial fit is here $0.76 \lambda^{1.7}$. The oscillations for $\lambda > 1$ get more and more suppressed with increasing frequency.

More precisely, we calculate the quantity $4 \det \rho_1(x)$, which is conjectured being a measure of the total entanglement, the site number x participates in [29]. For three qubits, the difference between this quantity and the sum of all squared concurrences with site number x is the 3-tangle, a measure for pure-state three-site entanglement. The results are shown in Fig. 13. For $\gamma = 0.1$ (upper panel) the result is qualitatively very similar to that found for the concurrence: there is an entanglement wave, propagating with velocity λ . However, for higher γ 's, such wave is characterized by a much larger average value. As we shall see, this is an effect of entanglement dynamically generated from the vacuum. In order to get an idea of what part of the signal for the total entanglement (referring to the conjecture on the amount of residual entanglement, Ref. [29]) comes from the singlet, we are next having a look at the total entanglement created solely from the vacuum, i.e. the initial state being the vacuum. The results are shown in figure 14. For the XY model, the vacuum signal identically vanishes.

For *small anisotropy* ($\gamma = 0.1$) the entanglement from the vacuum is negligible and it increases abruptly for λ being considerably near to the critical coupling; beyond this point, strong oscillations appear. For *medium anisotropy* the amplitude of the oscillations for $\lambda > 1$ is suppressed and their frequency increases. The created entanglement smoothly increases until the critical λ . At $\gamma = 1$ a plateau is rapidly reached at $\lambda = 1$ and the oscillations are severely suppressed.

For different γ we see that the average entanglement increases for $\gamma \rightarrow 1$, whereas the relative amplitude of its oscillation decreases. It is worth noticing that the average entanglement is reached on extremely short timescales, which decrease with increasing γ .

We then analyzed the evolution of the singlet onto the vacuum. Sufficiently far away from the local perturbation and for sufficiently short time we expect that the entanglement observed should be mainly that of the underlying vacuum. Whereas notable deviations should be observed close to the propagating concurrence.

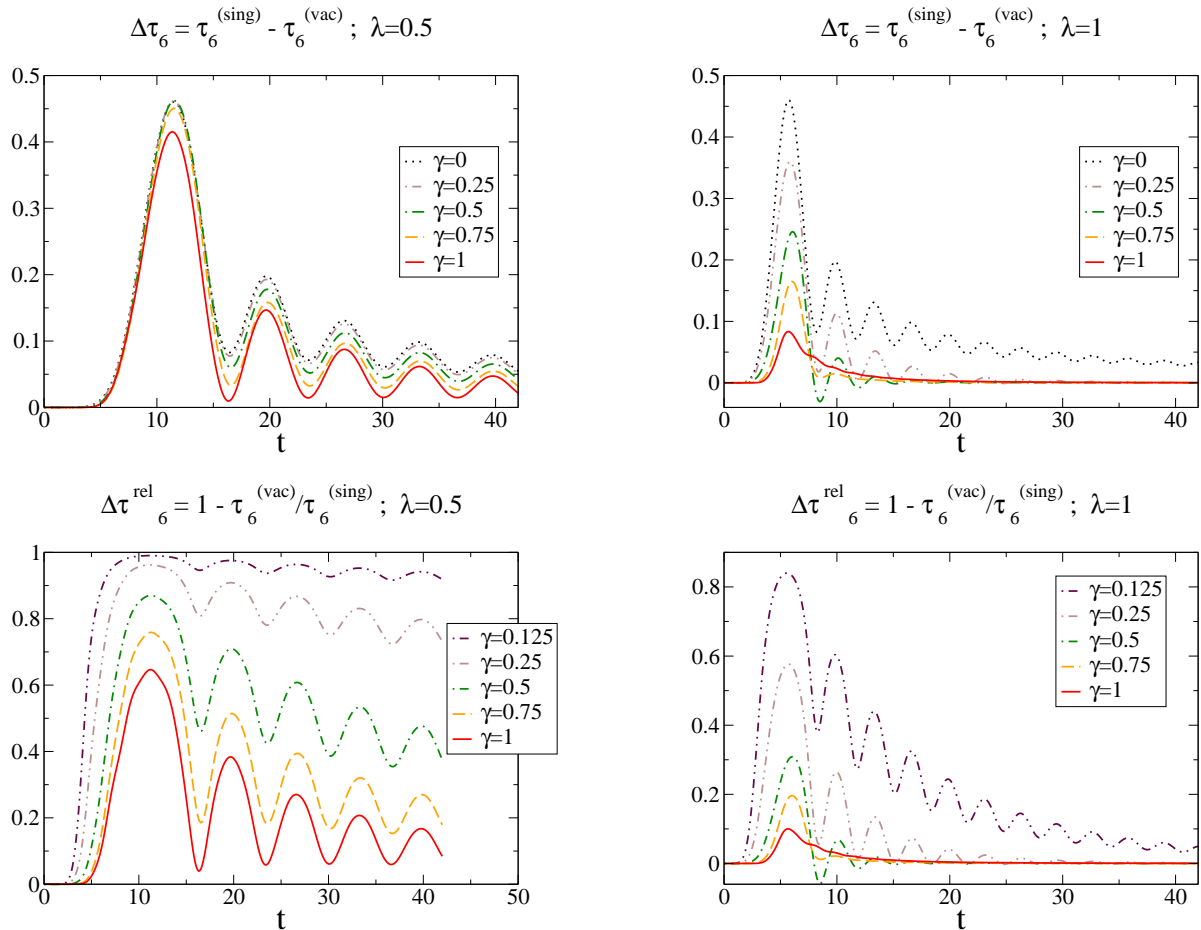


FIG. 15. The tangle deviation $\Delta\tau_6$ (upper panel) and the relative tangle deviation $\Delta\tau_6^{\text{rel}}$ from the Vacuum tangle at site number 6 for different values of γ for a fixed value of λ : $\lambda = 0.5$ (left) and $\lambda = 1$ (right). It is nicely seen that the oscillation frequency does not depend on γ , but their damping does. The damping is enhanced at critical coupling $\lambda = 1$ due to the increasing relevance of the double spin-flips, which overwhelm the singlet propagation.

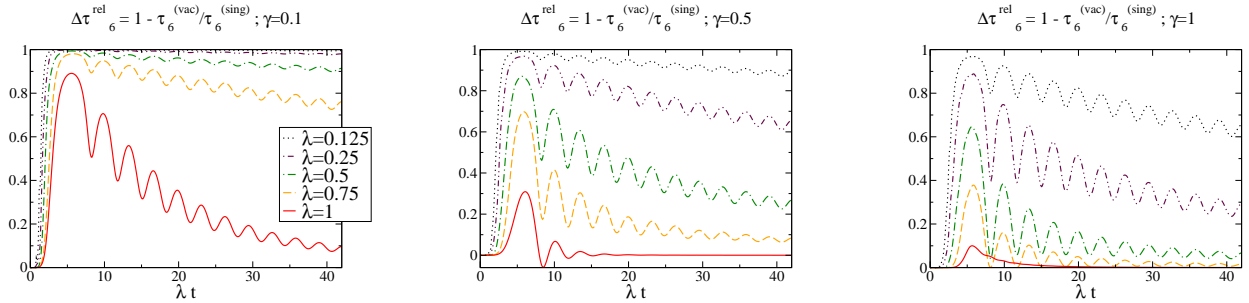


FIG. 16. The relative tangle deviation $\Delta\tau_6^{rel}$ from the Vacuum tangle at site number 6 for different values of λ for a fixed value of γ : $\gamma = 0.1$ (left), $\gamma = 0.5$, and $\gamma = 1$ (right). It is plotted as a function of the reduced time $\tau = t/\lambda$; it is nicely seen that the oscillation frequency grows linearly with λ .

In order to separate the deviations due to the propagating perturbation we subtract the global tangle emerging from the pure vacuum and study:

$$\Delta\tau_j := 4(\det \rho_j^{(1)} - \det \rho_{(vac)}^{(1)}) . \quad (47)$$

We want to stress that it is not a priori clear whether the time evolution operator preserves the relative order induced by the entanglement measures in the Hilbert space. It is visible in negative values of $\Delta\tau_j$ that this does not hold in general. Eventually, this is due to the fact that superposing (as well as mixing) orthogonal maximally entangled states of the same type diminishes the entanglement. This makes an “entanglement crossing” of the vacuum and the singlet possible, leading to a negative value of their difference. It is worth noticing that we insert the singlet state into the vacuum; this is not a superposition of the vacuum and some other state.

Below the critical λ , $\Delta\tau_j$ increases slightly with decreasing γ but looks very similar for different values of γ . It slowly tends to zero (left-upper part of Fig. 15). At the critical coupling $\lambda = 1$ we observe immediate convergence to zero for large enough t , (right-upper part of Fig. 15). This is much in contrast to the isotropic case, $\gamma = 0$, which is also shown in the upper rightmost plot in Fig. 15. This could indicate that at the critical coupling, though being in an excited state, the residual tangle be mainly originated by global properties of the initial state. A notable contribution from the singlet is found at very small t , which gets even smaller when λ increases. It is only for small up to medium λ , that the singlet contribution survives much longer. The data is consistent with the propagation velocity being λ , independent of γ (Fig. 15).

The surprising similarity of the difference signal for much different γ (upper panel of Fig.15) disappears when looking at the relative deviation, i.e. $\Delta\tau_j^{rel} := 1 - \det \rho_{(vac)}^{(1)} / \det \rho_j^{(1)}$ (lower panel of Fig. 15; Fig.16). We choose the same parameter range as above. Along the axis $t = 0$ and $\lambda = 0$ and for site numbers larger than two (and smaller than one) we have that $\det \rho_j^{(1)} = 0$. In these cases, also $\det \rho_{(vac)}^{(1)} = 0$, and we chose the plotted

value being zero in these cases. The analysis of $\Delta\tau_j^{rel}$ tells us that for small anisotropy and sufficiently far from the critical coupling the global tangle is dominated by the local perturbation of the vacuum by the singlet (lower-left plot in Fig. 15). Meaning also that the total tangle is concurrence dominated. For the isotropic XY model, the global tangle was given entirely by the sum of the 2-tangles such that the CKW-conjecture would conclude that there is no higher tangle contained in the system. In the presence of a small anisotropy, this is no longer true, in particular near to the critical coupling $\lambda = 1$ (lower-right plot in Fig. 15). Cranking up the anisotropy enhances the vacuum domination as well as tuning $\lambda \rightarrow 1$.

D. $\gamma \neq 0$: Singlet onto the ground state

1. Singlet-type perturbation of the groundstate

One could ask the critical question, whether or not the results in the preceding sections were specific to the vacuum state or what would happen for different states. We discuss in this section the propagation of a singlet-like perturbation onto the groundstate $|GS\rangle$. With *singlet-like perturbation* we mean to study the time evolution of the initial state

$$|S\rangle_g := \frac{1}{\sqrt{2}}(c_1 - c_2) |GS\rangle . \quad (48)$$

We note that this state differs from a singlet (i.e. a fully entangled state on the sites one and two – see appendix C for details) since the operators c_i create global (rather than local) excitations. For the isotropic model $|GS\rangle \equiv |\uparrow\uparrow\rangle$ and hence the dynamics is the same as on the vacuum. An indicator for how far away is the ground state for general $\gamma > 0$ from $|\uparrow\uparrow\rangle$ is, how much the norm of $|S\rangle_g$ differs from 1. We observed that notable deviations from 1 are present either for critical coupling at any $\gamma > 0$ or for non-critical coupling when γ is larger than about $1 - \lambda$. For $\lambda < 1$ at maximum 10% of the weight is lost. The situation changes drastically for $\lambda > 1$, where

for all $\gamma > 0$ we have a weight-loss of about 50%. We further want to note that the correspondence between fermion creation operators and spin raising operators (established by the Jordan-Wigner transformation) is different for the state $|\uparrow\rangle$ and the vacuum $|\downarrow\rangle$. Acting on the state $|\downarrow\rangle$ it is $S_i^+ = c_i^\dagger$; for the state $|\uparrow\rangle$ we have instead $S_i^+ = (-1)^{(i-1)}c_i^\dagger$.

Apart from the propagation of the pulse, which again goes with a velocity about λ , there are many qualitative differences for the concurrence. One of them is that the propagating pulse and the initial Bell state on sites 1 and 2 is the triplet with zero magnetization (figure 18). The concurrence plots (Fig. 20) show that the initial state, $|S\rangle_g$, is almost fully entangled on sites 1 and 2. This demonstrates how close is the ground state to $|\uparrow\rangle$. Two new features appears in the concurrence signal. Firstly, the entanglement pulse propagates on top of a nonzero background level, which in very good agreement coincides with the nearest neighbor concurrence of the ground state, being around 0.2 at both the critical point (see Fig. 20) and $\gamma = 0.5$ [18]. This shows that not only is the ground state very close to the vacuum, but that also

the state $|S\rangle_g$ is very similar to the ground state as far as nearest neighbor concurrence is considered. Secondly, in contrast to the singlet on the vacuum, we here have to deal with a propagation that eliminates the background concurrence. The latter feature gets more pronounced when approaching the Ising model and critical coupling (see Fig. 17). This elimination is understood from the fact that joining entanglement of the same type (here: two-site entanglement) in form of states that are orthogonal to those forming the entanglement already present, diminishes the entanglement; in fact, the fidelity plots demonstrate that the background entanglement is of the type $|\uparrow\uparrow\rangle + |\downarrow\downarrow\rangle$, whereas the pulse is of the type $|\uparrow\downarrow\rangle + |\downarrow\uparrow\rangle$. Whereas here the impact of the propagating concurrence pulse coming from the initial 0-triplet is the stronger the closer we get to the critical coupling and the quantum Ising model (the opposite of what we observed for the initial singlet onto the vacuum), the situation would be the same as far as the total signal along the propagation line is concerned. This in fact gets more suppressed with growing λ and γ . For γ tending to zero the ground state tends to $|\uparrow\rangle$, and hence we have the same situation as for the isotropic model.

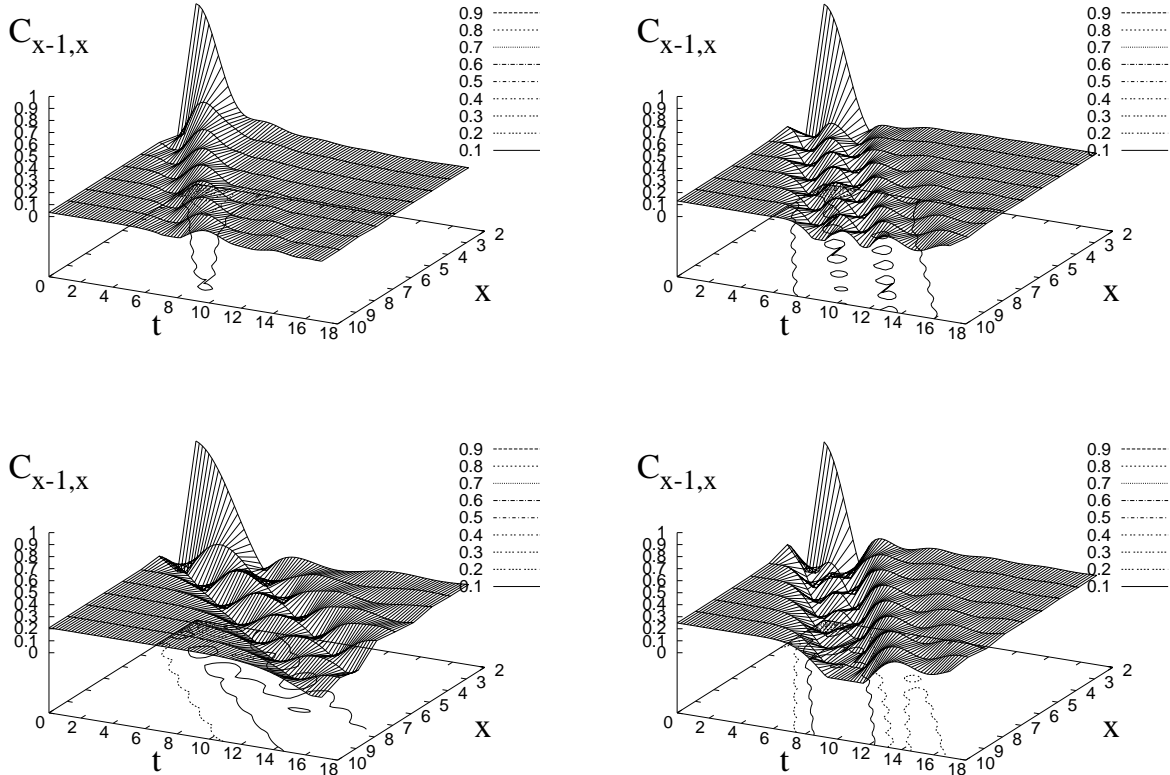


FIG. 17. The nearest neighbor concurrence for different λ and γ . *Upper panel*: $\gamma = 0.1$ (left) and $\gamma = 0.5$ (right) for critical coupling $\lambda = 1$. *Lower panel*: Ising model ($\gamma = 1$) for $\lambda = 0.5$ (left) and $\lambda = 0.9$ (right). It is seen that instead of the enhancement of concurrence at short times, we here have a background concurrence corresponding to the ground state value (see Fig. 20 in appendix D). The propagating signal is seen on top of a valley of extinction.

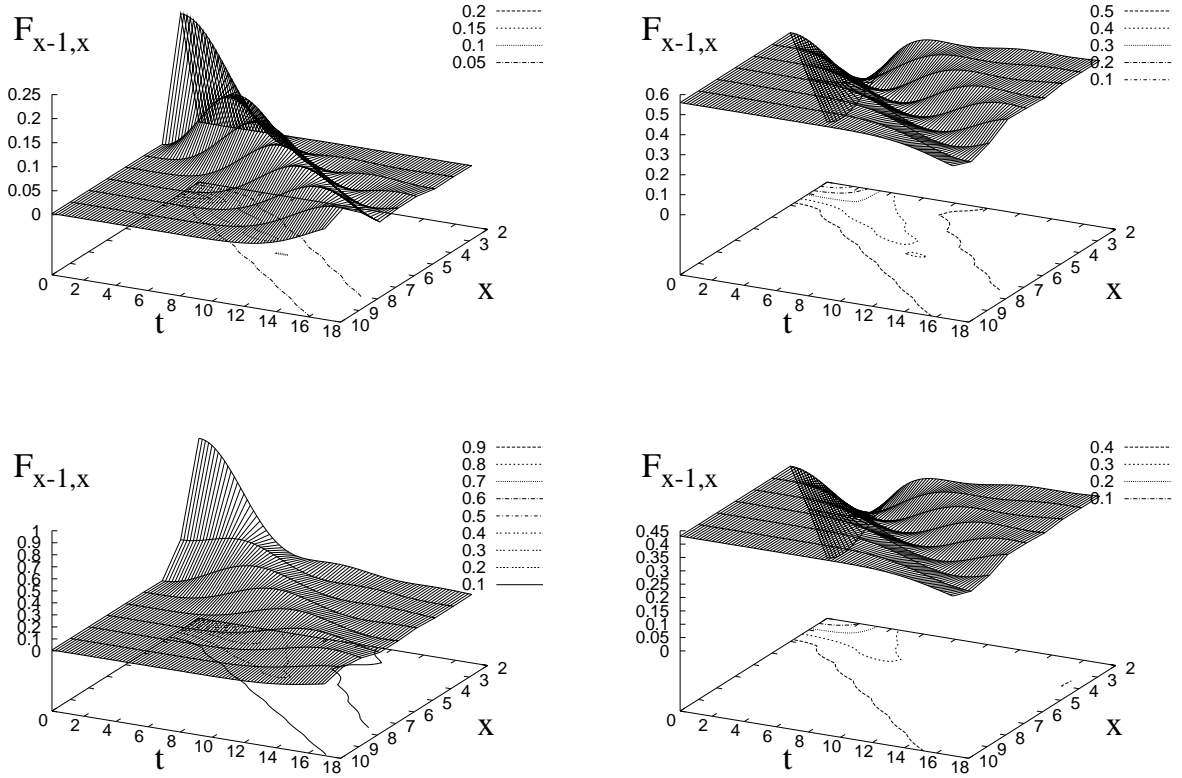


FIG. 18. The fidelity for the Bell states in the reduced density matrix is drawn for $\gamma = \lambda = 0.5$; the initial state is a singlet type perturbation on top of the ground state. Since an equal mixture of two Bell states is a disentangled state, the pictures show that the predominant Bell state in the background entanglement is the triplet $1/\sqrt{2}(|\uparrow\uparrow\rangle + |\downarrow\downarrow\rangle)$ (upper rightmost picture). For the propagation the situation is opposite to what was found for the singlet on top of the vacuum: the propagation is dominated by the zero triplet (lower leftmost picture) and not the singlet but the singlet seems to decay more slowly such that it eventually could become dominant.

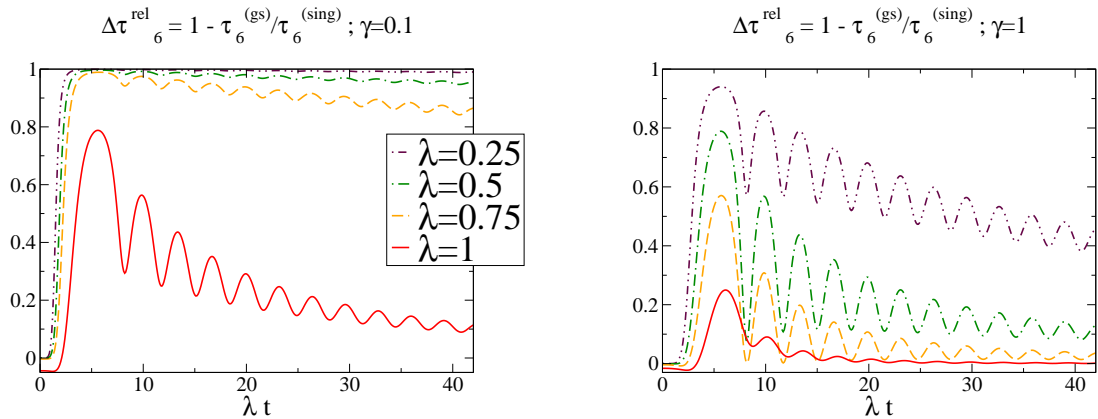


FIG. 19. The relative tangle deviation $\Delta\tau_6^{rel}$ from the ground state tangle at site number 6 for different values of λ for a fixed value of γ : $\gamma = 0.1$ (left) and $\gamma = 1$ (right). It is plotted as a function of λt ; it can be seen that the oscillation frequency grows linearly with λ .

For the global tangle we find essentially the same behavior as for the singlet on the vacuum. Only at very short times the singlet-type perturbation diminishes the global tangle. In Fig 19 we choose two different

anisotropies $\gamma = 0.1$ and 1 and compare $\Delta\tau_j^{rel}$ for different couplings λ . In a preliminar analysis, the short-time behavior of $\Delta\tau_6^{rel}$ shows a marked anomaly at the critical coupling that will be discussed elsewhere.

V. CONCLUSIONS

In the present work we studied the effect of a singlet-type perturbation on the entanglement of an infinite spin system. We considered quantum XY models for general anisotropy. The dynamics of entanglement was studied as function of the distance to the local perturbation at $t = 0$, and of the reduced interaction strength λ (up to the common quantum critical point of the models at $\lambda = 1$). For this class of models we analyzed a conjecture formulated by Coffman, Kundu, and Wootters quantifying the weight of the pairwise relatively to the global entanglement, measured by $4 \det \rho_1$.

The isotropic model, i.e. anisotropy $\gamma = 0$, can be mapped onto a tight binding model, and consequently entanglement propagates only, remaining pairwise; the velocity of the propagation is λ . A nearest neighbor entanglement at $t = 0$ not only propagates in both directions, remaining of type nearest neighbor; in addition, there is a notable concurrence signal between the sites with distance $\pm\lambda t$ to the initial Bell state at time t (see Fig. 3). This phenomenon can be interpreted as the production of an EPR pair: the initial Bell state splits into parts moving with the same velocity λ in opposite directions of the chain. We found that singlet-like states are transmitted after a crossing with higher fidelity than other maximally entangled states in the sense that the latter tend to switch into a singlet if the crossing involves a single site only. The global tangle and the concurrence (whose square is the 2-tangle) satisfy the Coffman-Kundu-Wootters conjecture with zero residual tangle. This means that *the system contained only pairwise entanglement, measured by the concurrence*. The Hamiltonian does not create any entanglement; it distributes the initially created pairwise entanglement.

For general anisotropy γ we inserted a singlet at $t = 0$ in the state $|\downarrow\rangle$. Also in this case we found the propagation of entanglement with velocity λ together with the evidence for an EPR-type propagation (see Fig. 12). The propagation is predominantly of the type $(|\uparrow\downarrow\rangle - |\downarrow\uparrow\rangle)$ as is the initial perturbation at $t = 0$. A triplet state $|\uparrow\downarrow\rangle + |\downarrow\uparrow\rangle$ is also present; it seems to decay more slowly than the singlet, indicating an eventual swap, as the system evolves, of the singlet into a triplet (see Fig. 11). The propagation is suppressed, compared to the isotropic model. The suppression is stronger the closer the system is to the critical coupling and the quantum Ising model (Fig.10). For the latter we found a very rapid damping of the singlet in the nearest neighbor concurrence. For all larger distances we considered (up to 7 lattice spacings) the concurrence is zero (in the range of the plots). A peculiarity of the anisotropic models is the instantaneous creation of concurrence from the vacuum all over the chain. This concurrence is due to the presence of pairwise spin-flips $s_j^+ s_{j+1}^+$ and $s_j^- s_{j+1}^-$ and results to be of

triplet type. It decays very quickly when approaching the quantum critical coupling and getting close to the Ising model. Neither effect is of critical origin, though. Comparing quantitatively $4 \det \rho_1$ and concurrence we could conclude that *for the anisotropic model the propagation of the concurrence is a small effect respect to the creation of the global tangle*. This indeed becomes more and more dominant when approaching the Ising model and the critical point (Fig.13). Medium interaction strengths and/or small anisotropy favor the propagation of the singlet.

We also studied the time evolution of a singlet-type perturbation of the ground state. We notice that though the perturbation has the form of a singlet, the initial state is the triplet $|\uparrow\downarrow\rangle + |\downarrow\uparrow\rangle$ (see Fig 18). Consequently, the propagation involves states of this type; the propagation velocity is still λ but the concurrence signal occurs along a “valley” in the constant background concurrence (Fig. 17). The propagation of the nearest neighbor concurrence (in form of an extinction) gets more enhanced with growing anisotropy and approaching the critical coupling; very much the contrary of what we found for the singlet on the vacuum. For the critical Ising model we found immediate extinction of the initial nearest neighbor concurrence but the valley with a weak propagating signal in it remains. The background nearest neighbor concurrence coincides with that of the ground state, indicating that the nearest neighbor concurrence distant from the initial perturbation is unaffected. The all over creation of entanglement is absent, suggesting that the Hamiltonian cannot create nearest neighbor concurrence on top of that already present in the underlying ground state.

Since the ground state is a highly correlated state, a locally created singlet on the wavefunction modifies the system over a long range. Nevertheless, the dynamics of the total tangle is basically unchanged (with respect to the vacuum case), differing only in minor quantitative details. In the short-time behavior of $\Delta_{T_x}^{rel}$ we observed an interesting anomaly at the critical coupling that needs to be addressed further.

We would like to mention finally that understanding the dynamics of entanglement may be relevant to characterize the behaviour of quantum registers. The information encoded in a given register can be lost either because of decoherence or if (unintentionally) the state of the register is not an eigenstate of the Hamiltonian. In the latter case, the residual dynamics will let the encoded state evolve in time. Due to the spin interactions, fidelity and the amount of entanglement will consequently vary in time.

In this work we consider exclusively ordered systems, and the role of imperfections is studied elsewhere [45].

ACKNOWLEDGMENTS

The authors would like to thank G. Falci and J. Siewert for helpful discussions. This work was supported by

APPENDIX A: PFAFFIANS

In this appendix, in order to make the presentation self-contained, we review the results obtained in [36]

$$\langle S_l^\alpha S_{l+R}^\beta \rangle = s(\alpha, \beta) \text{pf} \begin{vmatrix} I_{1,2}^{\alpha\beta} & \cdots & I_{1,R-1}^{\alpha\beta} & J_1^{\alpha\beta} & F_1^{\alpha\beta} & G_{1,2}^{\alpha\beta} & \cdots & \cdots & G_{1,R}^{\alpha\beta} \\ \cdots & \cdots & \cdots & \cdots & \cdots & \cdots & \cdots & \cdots & \cdots \\ & & I_{R-2,R-1}^{\alpha\beta} & J_{R-2}^{\alpha\beta} & F_{R-2}^{\alpha\beta} & G_{R-2,2}^{\alpha\beta} & \cdots & \cdots & G_{R-2,R}^{\alpha\beta} \\ & & & J_{R-1}^{\alpha\beta} & F_{R-1}^{\alpha\beta} & G_{R-1,2}^{\alpha\beta} & \cdots & \cdots & G_{R-1,R}^{\alpha\beta} \\ & & & & E^{\alpha\beta} & D_2^{\alpha\beta} & \cdots & \cdots & D_R^{\alpha\beta} \\ & & & & & K_2^{\alpha\beta} & \cdots & \cdots & K_R^{\alpha\beta} \\ & & & & & & H_{2,3}^{\alpha\beta} & \cdots & H_{2,R}^{\alpha\beta} \\ & & & & & & \cdots & \cdots & \cdots \\ & & & & & & & & H_{R-1,R}^{\alpha\beta} \end{vmatrix} \quad (\text{A1})$$

where $s(x, x) = s(y, y) = 1/4(-)^{R(R+1)/2}$,

$$\begin{aligned} I_{\mu,\nu}^{xx} &= \langle A_{l+\mu}(t) A_{l+\nu}(t) \rangle \\ J_\mu^{xx} &= I_{\mu,R}^{xx} \end{aligned} \quad (\text{A2})$$

$$\begin{aligned} H_{\mu,\nu}^{xx} &= \langle B_{l+\mu-1}(t) B_{l+\nu-1}(t) \rangle \\ K_\nu^{xx} &= H_{1,\nu}^{xx} \end{aligned} \quad (\text{A3})$$

$$\begin{aligned} G_{\mu,\nu}^{xx} &= \langle A_{l+\mu}(t) B_{l+\nu-1}(t) \rangle \\ F_\mu^{xx} &= G_{\mu,1}^{xx} \\ E^{xx} &= G_{R,1}^{xx} \\ D_\nu^{xx} &= G_{R,\nu}^{xx} \end{aligned}$$

$$\begin{aligned} I_{\mu,\nu}^{yy} &= \langle A_{l+\mu-1}(t) A_{l+\nu-1}(t) \rangle \\ J_\mu^{yy} &= I_{\mu,R}^{yy} \end{aligned} \quad (\text{A4})$$

$$\begin{aligned} H_{\mu,\nu}^{yy} &= \langle B_{l+\mu}(t) B_{l+\nu}(t) \rangle \\ K_\nu^{yy} &= H_{1,\nu}^{yy} \end{aligned} \quad (\text{A5})$$

$$\begin{aligned} G_{\mu,\nu}^{yy} &= \langle A_{l+\mu-1}(t) B_{l+\nu}(t) \rangle \\ F_\mu^{yy} &= G_{\mu,1}^{yy} \\ E^{yy} &= G_{R,1}^{yy} \\ D_\nu^{yy} &= G_{R,\nu}^{yy} \end{aligned}$$

and $s(x, y) = s(y, x) = -i/4(-)^{R(R-1)/2}$,

the EU (IST-SQUBIT), RTN2-2001-00440, HPRN-CT-2002-00144.

where the out of equilibrium correlation functions are calculated exactly, expressed as an expansion of pfaffians. The pfaffian for the ‘‘vacuum’’ expectation is defined as follows

$$\begin{aligned} I_{\mu,\nu}^{xy} &= \langle A_{l+\mu}(t) A_{l+\nu}(t) \rangle \\ G_{\mu,\nu}^{xy} &= \langle A_{l+\mu}(t) B_{l+\nu}(t) \rangle \end{aligned} \quad (\text{A6})$$

$$\begin{aligned} J_\mu^{xy} &= G_{\mu,0}^{xy} \\ F_\mu^{xy} &= G_{\mu,1}^{xy} \end{aligned} \quad (\text{A7})$$

$$\begin{aligned} H_{\mu,\nu}^{xy} &= \langle B_{l+\mu}(t) B_{l+\nu}(t) \rangle \\ E^{xy} &= H_{0,1}^{xy} \\ D_\nu^{xy} &= H_{0,\nu}^{xy} \\ K_\nu^{xy} &= H_{1,\nu}^{xy} \end{aligned} \quad (\text{A8})$$

$$\begin{aligned} I_{\mu,\nu}^{yx} &= \langle A_{l+\mu-1}(t) A_{l+\nu-1}(t) \rangle \\ G_{\mu,\nu}^{yx} &= \langle A_{l+\mu-1}(t) B_{l+\nu-1}(t) \rangle \end{aligned} \quad (\text{A9})$$

$$\begin{aligned} J_\mu^{yx} &= I_{\mu,R}^{yx} \\ F_\mu^{yx} &= I_{\mu,R+1}^{yx} \end{aligned} \quad (\text{A10})$$

$$\begin{aligned} E^{yx} &= I_{R,R+1}^{yx} \\ D_\nu^{yx} &= G_{R,\nu}^{yx} \end{aligned} \quad (\text{A11})$$

$$\begin{aligned} K_\nu^{yx} &= G_{R+1,\nu}^{yx} \\ H_{\mu,\nu}^{yx} &= \langle B_{l+\mu-1}(t) B_{l+\nu-1}(t) \rangle \end{aligned}$$

In the case in which the expectation value is taken over the ‘‘vacuum state’’ $|\Downarrow\rangle$, the two point correlators are

$$\begin{aligned} \langle \Downarrow | A_l(t) B_{l+R}(t) | \Downarrow \rangle &= \delta_{R,0} \\ &- \frac{2}{L} \sum_k [\cos(kR) (u_k^o)^2 + \sin(kR) u_k^e u_k^o] \end{aligned} \quad (\text{A12})$$

$$\langle \Downarrow | A_l(t) A_{l+R}(t) | \Downarrow \rangle = \delta_{R,0} - i \frac{2}{L} \sum_k \sin(kR) u_k^o v_k \quad (\text{A13})$$

$$\langle \Downarrow | B_L(t) B_{L+R}(t) | \Downarrow \rangle = - \langle \Downarrow | A_L(t) A_{L+R}(t) | \Downarrow \rangle^* \quad (\text{A14})$$

where

$$u_k^o = \lambda \gamma \sin k \frac{\sin(\Lambda_k t)}{\Lambda_k} \quad (\text{A15})$$

$$u_k^e = (1 + \lambda \cos k) \frac{\sin(\Lambda_k t)}{\Lambda_k} \quad (\text{A16})$$

$$v_k = \cos(\Lambda_k t) \quad (\text{A17})$$

We point out that though the translational invariance is not broken, the Pfaffians do not reduce to determinants because $\langle \Downarrow | A_L(t) A_{L+R}(t) | \Downarrow \rangle \neq 0$.

APPENDIX B: CONCURRENCE FROM CORRELATION FUNCTIONS

The determination of the concurrence is related to the knowledge of the correlation functions of the model. We derive the structure of the two-qubit reduced density matrix $\rho^{(2)}$ for the model Hamiltonians (1). These Hamiltonians have all the same quantum critical point (except for the XY model at $\gamma = 0$) and are solved exactly [30–32]. Certain symmetries of the Hamiltonian could restrict the structure of the reduced density matrix as long as they are not broken.

$$\rho^{(2)} = \begin{pmatrix} \frac{1}{4} + M_z + g_{zz} & 0 & 0 & g_{xx} - g_{yy} - i(g_{xy} + g_{yx}) \\ 0 & \frac{1}{4} - g_{zz} + \delta S_z & g_{xx} + g_{yy} + i(g_{xy} - g_{yx}) & 0 \\ 0 & g_{xx} + g_{yy} - i(g_{xy} - g_{yx}) & \frac{1}{4} - g_{zz} - \delta S_z & 0 \\ g_{xx} - g_{yy} + i(g_{xy} + g_{yx}) & 0 & 0 & \frac{1}{4} - M_z + g_{zz} \end{pmatrix} \quad (\text{B3})$$

giving for the concurrence (B2)

$$C = 2 \max \left\{ 0, \sqrt{(g_{xx} - g_{yy})^2 + (g_{xy} + g_{yx})^2} - \sqrt{\left(\frac{1}{4} - g_{zz}\right)^2 - \delta S_z^2}, \sqrt{(g_{xx} + g_{yy})^2 + (g_{xy} - g_{yx})^2} - \sqrt{\left(\frac{1}{4} + g_{zz}\right)^2 - M_z^2} \right\}. \quad (\text{B4})$$

For states with translational invariance $\delta S_z = 0$, i.e. $x = y$ in Eq. (B1), and in the presence of reflection symmetry, $g_{xy} = g_{yx}$, leading to real z in Eq. (B1). As far as eigenstates of the Hamiltonians are concerned, all above symmetries are present, making g_{xy} vanish, and

1. The generic case

The symmetries that can be used to simplify the form of $\rho^{(2)}$ are the *translational invariance*, the *reality* of the Hamiltonian and the *parity invariance*, meaning that the Hamiltonian can either leave the value of S_z unchanged or change it in steps of 2. For periodic boundary conditions, which we will consider here, we also have a reflection symmetry with respect to a mirror along a diameter of the ring. The parity invariance is spontaneously broken in the ordered phase with $\langle S_x \rangle \neq 0$. We will consider states with unbroken symmetry only.

For states out of equilibrium with broken translational invariance, ρ_2 reflects only the parity invariance. Written in the basis $\{|\uparrow\uparrow\rangle, |\uparrow\downarrow\rangle, |\downarrow\uparrow\rangle, |\downarrow\downarrow\rangle\}$ it is

$$\rho^{(2)} = \begin{pmatrix} a & 0 & 0 & c \\ 0 & x & z & 0 \\ 0 & z^* & y & 0 \\ c^* & 0 & 0 & b \end{pmatrix}, \quad (\text{B1})$$

with real a, b, x, y , and complex c, z . The concurrence results to be

$$C = 2 \max\{0, C^{(1)}, C^{(2)}\}, \quad (\text{B2})$$

where $C^{(1)} = |c| - \sqrt{xy}$ and $C^{(2)} = |z| - \sqrt{ab}$. In terms of spin-spin correlation function, using the notations $g_{\alpha\beta} := \langle S_\alpha^1 S_\beta^2 \rangle$, $M_\alpha := \langle S_\alpha^1 + S_\alpha^2 \rangle / 2$, and $\delta S_\alpha := \langle S_\alpha^1 - S_\alpha^2 \rangle / 2$, (B1) becomes

we obtain in the equilibrium case

$$\Rightarrow \rho^{(2)} = \begin{pmatrix} a & 0 & 0 & c \\ 0 & x & y & 0 \\ 0 & y & x & 0 \\ c & 0 & 0 & b \end{pmatrix}, \quad a, b, c, x, y \in \mathbb{R} \quad (\text{B5})$$

Consequently the expression for the concurrence considerably simplifies in case of equilibrium to

$$C = 2 \max \left\{ 0, |g_{xx} - g_{yy}| - \frac{1}{4} + g_{zz}, \right. \\ \left. |g_{xx} + g_{yy}| - \sqrt{\left(\frac{1}{4} + g_{zz}\right)^2 - M_z^2} \right\}. \quad (\text{B6})$$

In order to calculate the entanglement of one site with the rest of the chain, we have to consider the one-site reduced density matrix. It is obtained from (B3)

$$\rho_j^{(1)} = \begin{pmatrix} \frac{1}{2} + \langle S_j^z \rangle & 0 \\ 0 & \frac{1}{2} - \langle S_j^z \rangle \end{pmatrix} \quad (\text{B7})$$

and the entanglement, the site number j participates in, is quantified by the 1-tangle

$$\tau_1[\rho_j^{(1)}] = 4 \det \rho_j^{(1)} = \frac{1}{4} - \langle S_j^z \rangle^2 \quad (\text{B8})$$

2. The isotropic model: $\gamma = 0$

Here the conservation of magnetization, or equivalently of the total number of particles, simplifies further the structure of the 2-site reduced density matrix $\rho^{(2)}$, if the initial state has a well-defined number of flipped spins. Written in the basis $\{|\uparrow\uparrow\rangle, |\uparrow\downarrow\rangle, |\downarrow\uparrow\rangle, |\downarrow\downarrow\rangle\}$ it is

$$\Rightarrow \rho^{(2)} = \begin{pmatrix} a & 0 & 0 & 0 \\ 0 & x & z & 0 \\ 0 & z^* & y & 0 \\ 0 & 0 & 0 & b \end{pmatrix}, \quad (\text{B9})$$

with real a, b, x, y , and complex z , which is Eq. (B1) for $c = 0$. The concurrence is then given by

$$C = 2 \max\{0, |z| - \sqrt{ab}\}, \quad (\text{B10})$$

because $|c| - \sqrt{xy}$ in Eq. (B2) is always negative here ($c = 0$).

For the case of the time evolution of a singlet (one of the Bell states, i.e. fully entangled) on top of the vacuum, which corresponds to a one-particle state, the structure of $\rho^{(2)}$ further simplifies to

$$\Rightarrow \rho^{(2)} = \begin{pmatrix} 0 & 0 & 0 & 0 \\ 0 & x & z & 0 \\ 0 & z^* & y & 0 \\ 0 & 0 & 0 & b \end{pmatrix} \quad (\text{B11})$$

with concurrence

$$C = 2|z|. \quad (\text{B12})$$

For an arbitrary one-particle state $\sum_j w_j |j\rangle$ one obtains

$$\rho_{r,s}^{(2)} = \begin{pmatrix} 0 & 0 & 0 & 0 \\ 0 & |w_r|^2 & w_r w_s^* & 0 \\ 0 & w_r^* w_s & |w_s|^2 & 0 \\ 0 & 0 & 0 & 1 - |w_r|^2 - |w_s|^2 \end{pmatrix}, \quad (\text{B13})$$

and consequently $C_{r,s} = 2|w_r w_s|$.

APPENDIX C: LOCAL SINGLET INSERTION INTO THE GROUNDSTATE

In order to place a singlet into an arbitrary state, it is in general inevitable to consider from the very beginning a density matrix rather than a pure state. We present the *knitting procedure* for the groundstate on the sites 1 and 2; the procedure nevertheless works for an arbitrary state (and of course for any two sites).

Defining

$$|\Phi_{\mu\nu}\rangle := |s\rangle \langle \mu\nu | GS \rangle, \quad (\text{C1})$$

with the singlet state

$$|s\rangle = 1/\sqrt{2}(|\uparrow\downarrow\rangle - |\downarrow\uparrow\rangle) = 1/\sqrt{2}(c_1^\dagger - c_2^\dagger)|\downarrow\downarrow\rangle.$$

They are realized by

$$\begin{aligned} \Phi_{\uparrow\uparrow} &= 1/\sqrt{2}(c_1^\dagger - c_2^\dagger)c_1 c_2 |GS\rangle \\ \Phi_{\uparrow\downarrow} &= 1/\sqrt{2}(c_1^\dagger - c_2^\dagger)c_1 c_2^\dagger |GS\rangle \\ \Phi_{\downarrow\uparrow} &= 1/\sqrt{2}(c_1^\dagger - c_2^\dagger)c_1^\dagger c_2 |GS\rangle \\ \Phi_{\downarrow\downarrow} &= 1/\sqrt{2}(c_1^\dagger - c_2^\dagger)c_1^\dagger c_2^\dagger |GS\rangle \end{aligned}$$

The density matrix one had to consider, is

$$\rho_{GS}^{singlet} := \sum_{\mu,\nu} |\Phi_{\mu\nu}\rangle \langle \Phi_{\mu\nu}| \quad (\text{C2})$$

and gives at $t = 0$ a fully entangled singlet state on the sites one and two and exactly the groundstate concurrence as long as the sites numbers 1 and 2 are not included. This is, because at $t = 0$

$$\text{tr}_{\{1,2\}} \rho_{GS}^{singlet} = \text{tr}_{\{1,2\}} |GS\rangle \langle GS|$$

i.e. the density matrix for the remaining $N - 2$ sites derived from $\rho_{GS}^{singlet}$, Eq. (C2), is identical to that one derived from the ground state itself. Consequently, all correlation functions are the same in both.

APPENDIX D: ADDENDUM FOR THE GROUND STATE

In this section we recall some of the results from Ref. [18] and add some that have not been explicitly presented there. In Fig. 20 the nearest neighbor concurrence for the ground state (infinite chain) is shown for different values of γ as a function of the reduced coupling λ . All these functions exhibit a logarithmic divergence

of the first derivative respect to λ at the quantum critical point $\lambda_c = 1$. For finite chains $\partial_\lambda C_1$ scales according to finite size scaling theory with the system size. This observation also applies to the first (non-zero) derivative of the concurrence for larger distances. The cusp, where C_1 vanishes is the point where the large eigenvalues of $R = \rho_{\sigma_y} \otimes \sigma_y \rho^* \sigma_y \otimes \sigma_y$ for the invariant sectors $|M_z| = 0$ and $|M_z| = 1/2$ are equal. This means that the the type

of Bell state responsible for the entanglement changes from one regime to the other. The invariance of these blocks is due to the parity symmetry. The value of λ where this degeneracy happens converges from above to the critical coupling $\lambda_c = 1$ for $\gamma \rightarrow 0$. Details will be discussed elsewhere. For the purpose of this work it is worth noticing that the groundstate values agree very well with the uniform background concurrence.

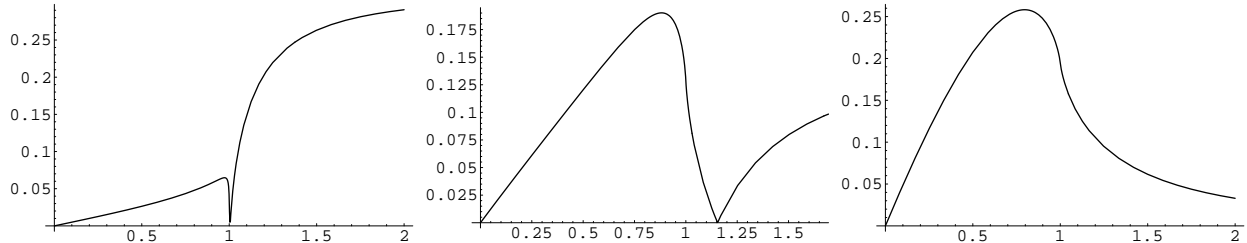
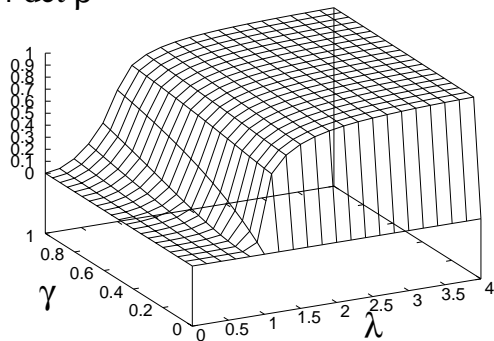


FIG. 20. The nearest neighbor concurrence C_1 for the values of $\gamma = 0.1, 0.5,$ and 1 from the left to the right. At $\lambda = 0.5$ and $\lambda = 1$, C_1 has roughly the same value: 0.0264 and 0.0337 for $\gamma = 0.1$, 0.1204 and 0.1285 for $\gamma = 0.5$; 0.2074 and 0.1946 for $\gamma = 1$, respectively. For the Ising model at $\lambda = 0.9$ (the coupling shown in Fig. 17) we have $C_1 = 0.2475$. These values appear as uniform background in the concurrence $C_1(x, t)$ for the singlet-type perturbation of the ground state (Fig. 17).

The one-tangle for the ground state is shown on the left of figure 21. This quantity was suggested to being an additive measure of entanglement [29] in the sense that the sum of all n -tangles (n from 2 to ∞) should give ex-

actly the one-tangle, being then the total entanglement present in the system (in the case of a translational invariant state, which is the ground state).

4 det ρ



CKW conjecture: Residual Tangle for $\lambda=1$

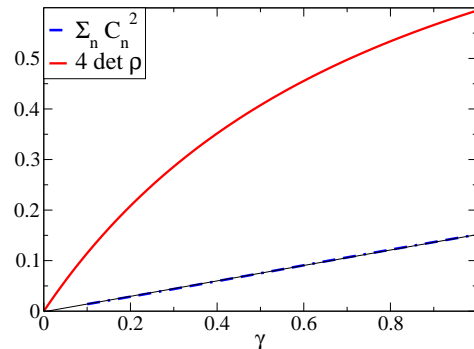


FIG. 21. The global tangle for the groundstate (left). For $0.1 \leq \gamma \leq 1$ we could verify the CKW conjecture for critical coupling (right). The one-tangle (thick line) is much larger than $\sum_n C_n^2$ (thick dash-dotted line) suggesting that the major part of entanglement should be stored in higher than two-qubit entanglement. The thin line is a guide to the eye showing that the sum of the two-tangles linearly tends to zero as $\gamma \rightarrow 0$.

At the critical point for $\gamma \in [0.1, 1]$ we could demonstrate that the sum of the two-tangles is much smaller than the one-tangle. The result is shown in the right plot of figure 21. If the CKW conjecture holds, this indicated that far the most entanglement is stored in higher

tangles (yet to be quantified). This indication recently found support in Ref. [20], where the scaling of the von Neumann entropy of a compact block of spins with the size of the block was studied.

-
- [1] J.S. Bell, *Speakable and unspeakable in Quantum Mechanics*, (Cambridge University Press, Cambridge, 1987).
- [2] M. Nielsen and I. Chuang, *Quantum Computation and Quantum Communication*, (Cambridge University Press, Cambridge, 2000).
- [3] A. Zeilinger, *Rev.Mod.Phys.***71**, 288,(1999).
- [4] A.Rauschenbeutel, G. Nogues, S. Osnaghi, P. Bertet, M. Brune, J.-M. Raimond, and S. Haroche, *Science*, **288**, 2024, (2000).
- [5] C.A.Sackett, D. Kielpinski, B. E. King, C. Langer, V. Meyer, C. J. Myatt, M. Rowe, Q. A. Turchette, W.M. Itano, D. J. Wineland, and C. Monroe, *Nature*, **404**, 256, (2000).
- [6] M. Bayer, P. Hawrylak, K. Hinzer, S. Fafard, M. Korkusinski, Z. R. Wasilewski, O. Stern, and A. Forchel, *Science* **291**, 451 (2001).
- [7] D. Loss and E.V. Sukhorukov, *Phys. Rev. Lett.* **84**, 1035 (2000); M.-S. Choi, C. Bruder, and D. Loss, *Phys. Rev. B* **62**, 13 569 (2000).
- [8] F. Plastina, R. Fazio, and G. M. Palma, *Phys. Rev. B* **64**, 113306 (2001).
- [9] S. Bose, quant-ph/0212041 (unpublished).
- [10] J. Preskill, *J. Mod. Optics* **47**, 127-137 (2000).
- [11] K.M. O’Connors and W.K. Wootters, *Phys. Rev. A* **63**, 052302 (2001).
- [12] X. Wang and P. Zanardi, *Phys. Lett. A* **301**, 1 (2002); X.Wang, *Phys. Rev. A* **66**, 034302 (2002).
- [13] R. F. Werner, *Phys. Rev. A* **40**, 4277 (1989).
- [14] X. Wang, *Phys. Rev. A* **64**, 012313 (2001).
- [15] M.C. Arnesen, S. Bose, and V. Vedral, *Phys. Rev. Lett.* **87**, 017901 (2001).
- [16] D. Gunlycke, S. Bose, V.M. Kendon, and V. Vedral, *Phys. Rev. A* **64**, 042302 (2001).
- [17] S. Sachdev, *Quantum Phase Transitions*, (Cambridge University Press, Cambridge, 2000).
- [18] A. Osterloh, L. Amico, G. Falci, and R. Fazio, *Nature* **416**, 608 (2002).
- [19] T. J. Osborne and M. A. Nielsen, *Phys. Rev. A* **66**, 044301 (2002).
- [20] G. Vidal, J. I. Latorre, E. Rico, A. Kitaev, *Phys. Rev. Lett.* **90**, 227902 (2003).
- [21] B.-Q.Jin and V.E.Korepin, quant-ph/0304108 (unpublished).
- [22] D. V. Khveshchenko, cond-mat/0301111, (unpublished).
- [23] P. Zanardi and X. Wang, *J. Phys. A*, **35**, 7947 (2002).
- [24] M.A. Martin-Delgado, quant-ph/0207026, (unpublished).
- [25] B. Zeng, H. Zhai, and Z. Xu, *Phys. Rev. A* **66**, 042324 (2002); A.P. Balachandran, L. Chandar, and Arshad Mo-
men, *Int. J. Mod. Phys. A* **12**, 625-642 (1997).
- [26] A. P. Hines, R. H. McKenzie, and G. J. Milburn, *Phys.Rev.A* **67**, 013609 (2003).
- [27] T.J. Osborne and M.A. Nielsen, quant-ph/0109024, (unpublished).
- [28] V. Giovannetti, S. Lloyd, and L. Maccone, *Phys. Rev. A* **67**, 052109 (2003); *ibid.*, *Europhys. Lett.* **62**, 615 (2003), and reference therein.
- [29] V. Coffman, J. Kundu, W. K. Wootters, *Phys.Rev. A* **61**, 052306 (2000).
- [30] E. Lieb, T. Schultz, D. Mattis, *Ann. Phys.* **60**, 407 (1961).
- [31] P. Pfeuty, *Ann. Phys. (N.Y.)*, *Ann. Phys.* **57**, 79-90 (1970).
- [32] E. Barouch, B.M. McCoy, and M. Dresden, *Phys. Rev. A*, **2**, 1075-1092 (1970); E. Barouch and B.M. McCoy, *Phys. Rev. A*, **3**, 786-804 (1971).
- [33] E. R. Caianello and S. Fubini, *Nuovo Cimento* **9**, 1218 (1952).
- [34] We would like to point out that the time dependence of the correlation functions calculated in Ref. [32] was due to a step-like time dependence in λ and the system was taken to be initially in equilibrium.
- [35] A further peculiarity of Eq.(12) as compared to the calculations done in Refs. [30–32] is that in the present case the Wick theorem leads to time dependent Pfaffians.
- [36] L. Amico and A. Osterloh, submitted to *J. Phys. A*.
- [37] G. Ghirardi, L. Marinatto, and T. Weber, *J. Stat. Phys.* **108**, 49 (2002).
- [38] The entropy of a block of L spins and the scaling of it as a function of L was discussed in Ref. [20]. Following the line of thought in Ref. [29], this quantity contained the more different types of entanglement the larger is L . We consider the case where A contains only a single site in order to study the conjecture in Ref. [29].
- [39] This relation can be found by noting the relation between the tangle and one of the eigenvalues λ of ρ_1

$$\lambda =: \frac{1}{2} \left(1 + \sqrt{1 - \tau_1[\rho_1]} \right).$$
- [40] W.K. Wootters, *Phys. Rev. Lett.* **80**, 2245-2248 (1998).
- [41] S. Hill and W. K. Wootters, *Phys. Rev. Lett.* **78**, 5022 (1997).
- [42] C.J. Bennett, H.J. Bernstein, S. Popescu, and B. Schumacher, *Phys. Rev. A* **53**, 2046-2052 (1996). V. Vedral, M.B. Plenio, M.A. Rippin, and P. Knight, *Phys. Rev. Lett.* **78**, 2275-2279 (1997). C.H. Bennett, D.P. DiVincenzo, J. Smolin, and W.K. Wootters, *Phys. Rev. A* **54**, 3824-3851 (1996).
- [43] We omit the indices n and m here, indicating that the considered Hilbert space consists of that two sites only.
- [44] This is in contrast to what should be observed, if the damping was related to the quantum critical point: it should depend on the size of the system in a way prescribed by the critical exponents of the system.
- [45] S. Montangero, G. Benenti, and R. Fazio (unpublished).